INTERNAL FLUID DYNAMICS WITHIN A NONSPINNING PARTIALLY LIQUID-FILLED SHELL DUE TO IMPOSED MOTION

PAUL WEINACHT
CHARLES L. NIETUBICZ

DECEMBER 1987

US ARMY BALLISTIC RESEARCH LABORATORY
ABERDEEN PROVING GROUND, MARYLAND

88 4 8 035

REPORT DOCUMENTATION PAGE

Form Approved
OMB No 0704-0188
Exp Date Jun 30, 1986

1a REPORT SECURITY CLASSIFICATION	1b. RESTRICTIVE MARKINGS
UNCLASSIFIED	AD A191 055

2a SECURITY CLASSIFICATION AUTHORITY	3 DISTRIBUTION/AVAILABILITY OF REPORT
	Approved for public release, distribution unlimited.
2b DECLASSIFICATION/DOWNGRADING SCHEDULE	

4 PERFORMING ORGANIZATION REPORT NUMBER(S)	5 MONITORING ORGANIZATION REPORT NUMBER(S)
BRL-TR-2880	

6a NAME OF PERFORMING ORGANIZATION	6b OFFICE SYMBOL (If applicable)	7a. NAME OF MONITORING ORGANIZATION
U.S. Army Ballistic Research Laboratory	SLCBR-LF	

6c. ADDRESS (City, State, and ZIP Code)	7b. ADDRESS (City, State, and ZIP Code)
Aberdeen Proving Ground, Maryland 21005-5066	

8a. NAME OF FUNDING/SPONSORING ORGANIZATION	8b OFFICE SYMBOL (If applicable)	9. PROCUREMENT INSTRUMENT IDENTIFICATION NUMBER

8c. ADDRESS (City, State, and ZIP Code)	10. SOURCE OF FUNDING NUMBERS			
	PROGRAM ELEMENT NO.	PROJECT NO.	TASK NO.	WORK UNIT ACCESSION NO
	62622A	1L162622A55	00	00

11. TITLE (Include Security Classification)
INTERNAL FLUID DYNAMICS WITHIN A NONSPINNING PARTIALLY LIQUID-FILLED SHELL DUE TO BURSTER RUPTURE

12 PERSONAL AUTHOR(S)
WEINACHT, PAUL and NIETUBICZ, CHARLES J.

13a TYPE OF REPORT	13b TIME COVERED	14. DATE OF REPORT (Year, Month, Day)	15. PAGE COUNT
Technical Report	FROM _____ TO _____		

16 SUPPLEMENTARY NOTATION

17	COSATI CODES		18. SUBJECT TERMS (Continue on reverse if necessary and identify by block number)
FIELD	GROUP	SUB-GROUP	
19	01		Liquid Filled Shells, Compressible Liquids
19	04		Fluid Mechanics,

19. ABSTRACT (Continue on reverse if necessary and identify by block number) This forced liquid projectile is being directed by the Munitions Branch of the U.S. Army Chemical Research, Development and Engineering Center (CRDEC). The Computational Aerodynamics Branch, Launch and Flight Division U.S. Army Ballistic Research Laboratory (BRL), has been tasked to determine the internal fluid dynamics within a partially liquid-filled shell subject to large rapidly applied pressures which result from internal burster tube rupture. The main area of concern is the determination of the time history of the internal pressure on the shell sidewalls and base.

A numerical model has been developed to simulate the internal fluid dynamics of this partially liquid-filled configuration. This numerical model solves the quasi one-dimensional Euler equations and a equation of state for liquid using the explicit MacCormack numerical technique. Results have been generated for an internal shell geometry currently being tested by the Terminal Ballistics Division (TBD), BRL. Comparisons are made between the numerically predicted pressure levels and the pressure measurements performed by TBD.

20 DISTRIBUTION/AVAILABILITY OF ABSTRACT	21 ABSTRACT SECURITY CLASSIFICATION
☒ UNCLASSIFIED/UNLIMITED ☐ SAME AS RPT ☐ DTIC USERS	UNCLASSIFIED

22a NAME OF RESPONSIBLE INDIVIDUAL	22b TELEPHONE (Include Area Code)	22c OFFICE SYMBOL
Paul Weinacht	(301) 278-4280	SLCBR-LF-R

DD FORM 1473, 84 MAR

83 APR edition may be used until exhausted
All other editions are obsolete

TABLE OF CONTENTS

LIST OF FIGURES

LIST OF FIGURES (Cont'd)

I. INTRODUCTION

The forced liquid project is being directed by the Munitions Branch of the U.S. Army Chemical Research, Development and Engineering Center (CRDEC). The Computational Aerodynamics Branch, Launch and Flight Division, U.S. Army Ballistic Research Laboratory (BRL) has been tasked to determine the internal fluid dynamics within a partially, liquid-filled shell subject to large rapidly applied pressures which result from internal burster tube rupture. The main area of concern is the determination of the time history of the internal pressure on the shell sidewalls and base.

Previously, an analytical technique had been developed for predicting the internal fluid dynamics of a partially liquid-filled, nonspinning cylinder subject to an impulsively applied pressure at one end.[1] While this analytical technique did highlight many of the important fluid dynamic processes which occur internally, the effect of important parameters such as the internal shell geometry and time dependence of the burster tube rupture pressure could not be considered.

Due to the difficulties in incorporating these parameters into an analytical model, a numerical model has been developed and is discussed in this report. This numerical model solves the quasi one-dimensional Euler equations and a equation of state for a liquid using the explicit MacCormack numerical technique. Results have been generated for an internal shell geometry currently being tested by the Terminal Ballistics Division (TBD), BRL.[2] Comparisons are made between the numerically predicted pressure levels inside the liquid filled shell and the pressure measurements performed by TBD.

II. NUMERICAL MODEL

A numerical model has been developed to simulate the internal fluid dynamics of a nonspinning partially liquid-filled shell due to burster tube rupture. In this section the numerical model is presented. First, a brief description of the configuration and the basic fluid dynamics is given; the governing equations and boundary conditions are then described; and finally the numerical procedure is outlined.

1. DESCRIPTION OF CONFIGURATION AND BASIC FLUID DYNAMICS

Figure 1 depicts the internal configuration being tested by the Terminal Ballistics Division and simulated in the current numerical model. The internal configuration is an ogive-cylinder-boattail with a central burster tube which extends axially from the nose. The axial dimension of the burster tube is approximately half the internal length of the shell. The wall of the burster tube has been purposely made weaker near the nose to control the location of burster tube rupture. The test configuration is aligned nose down, leaving some percentage of ullage (air space above the liquid) in the boattailed section of the shell, as shown in Figure 2.

The fluid, initially at rest, is set in motion when the burster tube ruptures due to the ignition of the propellant within the burster tube. The rupture of the burster tube subjects the surrounding liquid to a locally high pressure causing a pressure wave to propagate up the liquid, as shown in

1

Figure 2. This pressure wave propagates up the fluid and reflects from the liquid-air interface. After the reflection of the pressure wave from the liquid-air interface, the interface begins moving towards the shell base. A short time later the interface impacts on the base and another pressure wave is generated which propagates down the fluid inside the shell.

Several features of the fluid motion can be deduced from this proposed description of the fluid motion; (1) the compressible nature of the liquid is important, (2) the primary motion of the fluid is in the direction along the shell axis of symmetry, and (3) the interfaces which bound the fluid slug move as a result of the high pressure from the burster.

2. GOVERNING EQUATIONS

The motion of the fluid within the shell can be represented by the time-dependent, quasi one-dimensional Euler equations, shown in vector form below. This vector equation represents the equations of mass and momentum conservation along the axial direction within the shell; where ρ is the local fluid density, u is the axial fluid velocity, and P is the local fluid pressure. The internal area change within the shell is accounted for through the source term, $\vec{H}$, where A is the local cross sectional area of the shell.

$$\frac{\partial \vec{q}}{\partial t} + \frac{\partial \vec{F}}{\partial x} + \vec{H} = 0$$

$$\vec{q} = \begin{bmatrix} \rho \\ \rho u \end{bmatrix} \quad ; \quad \vec{F} = \begin{bmatrix} \rho u \\ \rho u^2 + P \end{bmatrix} \quad ; \quad \vec{H} = \begin{bmatrix} \frac{1}{A} \frac{\partial}{\partial x} \rho u \\ \frac{1}{A} \frac{\partial A}{\partial x} \rho u^2 \end{bmatrix} \tag{1}$$

Closure of this set of equations is accomplished using an equation of state for liquid,[3]

$$\frac{\partial P}{\partial \rho} = \frac{E}{\rho} \tag{2}$$

where E is the bulk modulus of the fluid. In using this equation of state, an isothermal process is assumed. A fluid bulk modulus of 320,000 psi is used throughout the computations.[4]

The equation of state can be incorporated within the equations of motion, yielding the following vector equation,

$$\frac{\partial \vec{q}}{\partial t} + \frac{\partial \vec{F}}{\partial x} + \vec{H} = 0 \quad .$$

$$\vec{q} = \begin{bmatrix} \rho \\ \rho u \end{bmatrix} \quad ; \quad \vec{F} = \begin{bmatrix} \rho u \\ \rho u^2 + E \ln \rho \end{bmatrix} \quad ; \quad H = \begin{bmatrix} \frac{1}{A} \frac{\partial A}{\partial x} \rho u \\ \frac{1}{A} \frac{\partial A}{\partial x} \rho u^2 \end{bmatrix} \tag{3}$$

Because this set of equations is to be solved on a grid (x,t) which moves with the fluid slug as a function of time, it is convenient to transform these equations into a computational space (ξ, t) which remains fixed in time and space. The resulting equations, after the transformation has been applied, are written below.

$$\frac{\partial}{\partial t}(q) + \frac{\partial}{\partial \xi}(\xi_t \, q + \xi_x \, F) + H = 0$$

where

$$\xi_t \equiv \frac{\partial \xi}{\partial t} = -x_t \, \xi_x \quad , \quad J = 1/x_\xi \qquad (4)$$

$$\xi_x \equiv \frac{\partial \xi}{\partial x} = J \quad , \quad x_\xi \equiv \frac{\partial x}{\partial \xi} \quad , \quad x_t \equiv \frac{\partial x}{\partial t}$$

$$q = \frac{1}{J}\, \vec{q} \quad , \quad F = \frac{1}{J}\, \vec{F} \quad , \quad H = \frac{1}{J}\, \vec{H} \quad .$$

3. BOUNDARY CONDITIONS

The governing equations discussed above describe the fluid motion inside the fluid domain. Using the quasi one-dimensional approach, the state of the fluid must also be specified at the two endpoints of the domain.

One of the domain endpoints is located at the location where the burster breaks. At this point the fluid is exposed to high pressure from the burster. This high pressure has been measured experimentally by TBD and is used in the numerical model to specify the pressure as a function of time at this endpoint in the computational domain. Using the equation of state, the first of the two dependent variables, the density, can be specified.

$$\rho(t) = \rho_0 \exp\,[P(t)/E] \qquad (5)$$

where ρ_0 is the liquid density at ambient conditions. The second dependent variable, ρu, can be obtained by applying the momentum equation.

At the other endpoint of the domain, the liquid-air interface, one of two sets of boundary conditions is applied depending of the state of the interface. The first set of boundary conditions is applied between the time the burster breaks and the liquid-air impacts on the shell base. Here, the pressure acting on the interface is nearly ambient, compared with the pressures produced by burster. Using the equation of state, the first of the two dependent variables, the density, can be specified,

$$\rho = \rho_0 \quad . \qquad (6)$$

3

The second dependent variable, ρu, can be obtained by applying the momentum equation.

The second set of boundary conditions is applied after the interface impacts on the shell base. The fluid is brought to rest locally, and the second dependent variable becomes zero at this endpoint in the fluid domain. The boundary condition for the density is obtained by applying the continuity (mass conservation) equation.

4. NUMERICAL PROCEDURE

The governing equations are solved using the second order accurate explicit MacCormack finite-difference numerical procedure.[5] The solution is obtained by dividing the computational domain into a number discrete intervals (or grid points) and the solution advanced in time using the following predictor-corrector approach.

Predictor

$$q_j^{\overline{N+1}} = q_j^N - \Delta t \left[(\xi_{tj} E_j^N - \xi_{tj-1} q_{j-1}^N) + \right. $$
$$\left. (\xi_{xj} E_j^N - \xi_{xj-1} E_{j-1}^N) + H^N \right] \tag{6a}$$

Corrector

$$q_j^{N+1} = \frac{1}{2} \left\{ q^{\overline{N+1}} + q_j^N - \Delta t \left[(\xi_{tj+1} q_{j+1}^{\overline{N+1}} - \xi_{tj} q_j^{\overline{N+1}}) \right. \right.$$
$$\left. \left. (\xi_{xj+1} E_{j+1}^{\overline{N+1}} - \xi_{xj} E_j^{\overline{N+1}}) + H^{\overline{N+1}} \right] \right\} \tag{6b}$$

where superscript "N" denotes the time level of the solution and the subscript "j" denotes the spacial location of the grid point.

Boundary conditions are updated at the predictor and corrector steps using the appropriate one sided spacial differencing. After the solution is updated, the updated position of the grid is determined by integrating the velocity of the grid endpoints in time.

The solutions presented in this report were obtained using 251 grid points and typically required 1750 time steps to span the time interval of interest. Each solution required approximately seven minutes of CPU time on a VAX 780 computer.

III. RESULTS

The results of the application of the numerical model are presented in two sections. The first section is concerned with validation of the numerical model, and comparisons are made between the numerical model and experimental

4

results obtained by TBD. In the second section, results of a parametric study examining the effect of ullage and the internal shell boattail angle are presented.

1. VALIDATION OF THE NUMERICAL MODEL

A total of 18 cases (various ullages and burster pressures histories) have been run using the numerical model and comparisons made with the experimental pressure data obtained by TBD to provide validation of the numerical model. Data from five of these cases are presented in this report. TABLE 1 displays the ullage for each of the five cases. In the experiments performed by TBD, the driving pressure produced by the burster was tailored by loading the burster with varying amounts of propellant. The amount of propellant used in each test is also shown in TABLE 1.

TABLE 1. Description of Cases.

Case ID	Ullage	Burster
FF3	10%	40gm
FF4	5%	40gm
FF5	3%	40gm
FF7	5%	50gm
FF11	5%	30gm

The TBD pressure data consists of output from five pressure gauges located inside the pressure vessel. The locations of four of these gauges is shown in Figure 3. The additional gauge (Gauge 1) is located inside the burster tube and does not provide information of interest to the current study. The pressure output from Gauge 2 is used to specify the pressure time-history at one endpoint in the fluid domain in the numerical model. The data from this gauge is numerically filtered before each computation to eliminate high frequency oscillations present in the experimental data. (In the results shown in this report only the Gauge 2 experimental data has been smoothed. Experimental data shown from the other gauges is the raw experimental data.)

Case FF5 is examined first in some detail to reconcile the physics with the experimental and numerical output. Results from the other cases follow a similar pattern. Figure 4a displays the experimental output of Gauge 2 and the smoothed data used as input to the numerical model. Figures 4b-4d show the experimentally measured and numerically predicted pressure at Gauges 3, 4 and 5 respectively, and reference to these figures is made repeatedly in the following several paragraphs. In order to aid in understanding the results in these figures, critical events have been marked on the graphs by alphabetic characters, and are referenced to in the text.

The event begins with the breakage of the burster tube. Gauge 2, which is near the location of burster rupture, experiences a rapid increase in pressure almost immediately. Two tenths of a millisecond later the primary pressure wave has propagated up the pressure vessel to Gauge 3(A), and at 0.35 milliseconds the pressure wave passes Gauge 4(B). The pressure wave continues to

5

propagate up the pressure vessel until it reaches the liquid-air interface. When the pressure wave reaches the liquid-air interface, an expansion wave is generated and begins propagating down the vessel. At the same time, the liquid-air interface is set in motion and begins moving towards the shell base. The liquid-air interface eventually impacts on the shell base, producing a large pressure rise at Gauge 5(C), and generates a compression wave which propagates down the pressure vessel. As this compression wave propagates through the boattailed portion of the vessel, the pressure behind the wave decreases with time. This is reflected in the drop in pressure at Gauge 5 following the large increase in pressure (D).

At this point in time there are primarily two waves propagating down the pressure vessel; an expansion wave propagating ahead of the compression wave. As the expansion wave reaches Gauge 4 (at about 0.5 milliseconds) (E), the pressure is relieved down to zero. A short time later, the compression wave passes Gauge 4 producing a large increase in pressure to nearly 40 kpsi (F). Between 0.65 and 0.75 milliseconds both of these waves pass Gauge 3(G).

Both the expansion and compression waves reach the pressurized surface of the fluid and reflect as compression and expansion waves respectively. Both of these waves propagate up the vessel, with the compression wave ahead of the expansion wave. As these waves pass Gauge 4 at about 1.0 milliseconds (H), a small increase in pressure due to the compression wave is observed, followed a large drop in pressure as the expansion wave passes Gauge 4. At 1.15 milliseconds the expansion wave has reached the shell base and the pressure is relieved back down to zero (I).

Pressure waves continue to cycle throughout the vessel, however the experimental results indicate that the internal pressure levels are significantly smaller once the pressure on the shell base has been relieved.

The internal fluid dynamics follow the same pattern in the other cases that were examined. Presented below are comparison of the experimental and numerical results for four additional cases in which the ullage and amount of burster propellant are varied.

Figures 5a and 5b show the experimental and numerical output from Gauges 4 and 5 for Case FF3. (No experimental data was obtained for Gauge 3 in this test.) The numerically predicted pressure time history is in good agreement with the experimental results for Gauge 4. The numerically predicted pressures at Gauge 5 are somewhat higher that the experimentally measured values. The arrival times of the waves are generally in good agreement. The relief of pressure on the base near the end of the event occurs slightly later in the numerical simulation than in the experiment.

The experimental and numerical results at Gauge 4 and 5 for Case FF4 are shown in Figures 6a and 6b. The pressures at Gauges 4 and 5 are somewhat underpredicted in the numerical analysis. The arrival times of the pressure waves are again predicted fairly well, except for the pressure wave which relieves the pressure on the shell base.

Figures 7a,b,c display the experimentally measured and computed pressures at Gauges 3, 4 and 5 for test FF7. The computed pressure history at Gauge 3 compares well with the experimental measurements. The numerical predictions

show that between 0.7 and 0.85 milliseconds the lower boundary of the fluid domain has been pushed past Gauge 3 by the burster gases. During this time period, high frequency oscillations in the experimental pressure trace are evident, which may suggest that experimentally the gauge is being exposed to the combustion gases from the burster tube. The computed and experimental pressure history at Gauge 4 are in fairly good agreement. The numerically predicted pressures at Gauge 5 are slightly greater than the experimental values and again the pressure relief on the shell base occurs later in the computation than in the experiment.

The pressure traces for Case FF11 are shown in Figures 8a,b,c. The computed pressures at Gauges 3 and 4 are again in good agreement with the experimental values. The computed pressures at Gauge 5 are significantly higher than the experimentally measured values, though the experimental results indicate negative pressures after 1.0 millisecond indicating a possible gauge zero-drift problem.

In general, the numerical results show excellent agreement with the experimental results at Gauge 3. This is not surprising due to the close proximity of Gauge 3 to Gauge 2, which is used as the driving pressure for the numerical model. The numerical results indicate that in a number of cases the lower liquid interface is pushed past gauge location 3, particularly as the ullage is increased. The numerical predictions of the pressure history at Gauge 4 are in good agreement with the experimental measurements. The numerical results at Gauge 5 display qualitatively the same features as does the experimental results. The arrival time of the fluid interface is well predicted and in many cases the pressures levels due to the impacting of the fluid interface on the base agree well with the experimental results. The eventual relief in pressure on the shell base occurs somewhat later in the computation than in the experiment, although this does not appear to be a critical parameter.

2. PARAMETRIC STUDY

One of the primary advantages of developing a numerical model, such as the one discussed here, is that parametric studies can be quickly and easily performed. The code developed in this study has been used to elicit the important parameters of the forced liquid problem. Two parameters examined here are the effects of ullage and boattail angle.

a. Ullage A parametric study examining the effect of ullage on the internal pressure history has been performed. Results have been generated for a single input pressure history (corresponding to Case FF5) and for several ullages; 3, 5, 10 and 15 percent.

Figures 9a and 9b show the pressure history at Gauge 3 for 5 and 10 percent ullages. For the first 0.6 milliseconds, the pressure history shows little variation between the two ullages. This was also observed in the computed results for 3 and 15 percent ullages. After 0.6 milliseconds, the numerical results show that the lower pressurized fluid surface is pushed past Gauge 3 for a duration of time that increases as the ullage increases. This behavior was observed in the computed results across the range of ullages examined.

7

The pressure histories at Gauge 5 for each of the ullages are shown in Figures 10a,b,c,d. The figures show that the base is generally exposed to higher pressures as the ullage is increased. However, the base experiences the pressure loading over a smaller duration as the ullage is increased.

b. Internal boattail angle A study was performed to demonstrate the effect of the internal boattail angle of the shell on the internal pressure history. Computations were performed for two boattail angles (7 and 10 degrees) using the FF5 input pressure, and a ullage of 10%.

The pressure history at Gauge 3 show very little variation due to the change in the internal boattail angle. The pressure history at Gauge 4, shown in Figure 11a, also show only small variations. The largest effect is noted at gauge location 5 (on the shell base) where larger peak pressures are predicted for the larger boattail angle, as shown in Figure 11b. The duration and average magnitude of the pressure loading are approximately the same.

IV. CONCLUSIONS

A quasi one-dimensional numerical model has been developed to compute the internal fluid dynamics of a nonspinning partially liquid-filled shell which results from burster tube rupture. Computational results have been obtained for a shell configuration currently being tested by TBD. The results show very good agreement when compared with pressure measurements obtained by TBD, validating the numerical approach. The numerical model has provided further insight into the physical processes which occur within the shell.

A parametric study has been performed using the numerical model to examine the effect of ullage and internal boattail angle of the shell on the internal surface pressures. The numerical results show that the fluid interface located in the vicinity of the burster tube rupture is pushed further from the nose of the shell by the high pressure gases as the ullage is increased. The results also show that the shell base is generally exposed to higher pressures as the ullage is increased, however, the base experiences these higher pressures over a somewhat shorter duration. The numerical results show that as the boattail angle of the shell is increased the peak base pressures are increased, though the average pressure and the duration of the pressure load on the shell base remain constant.
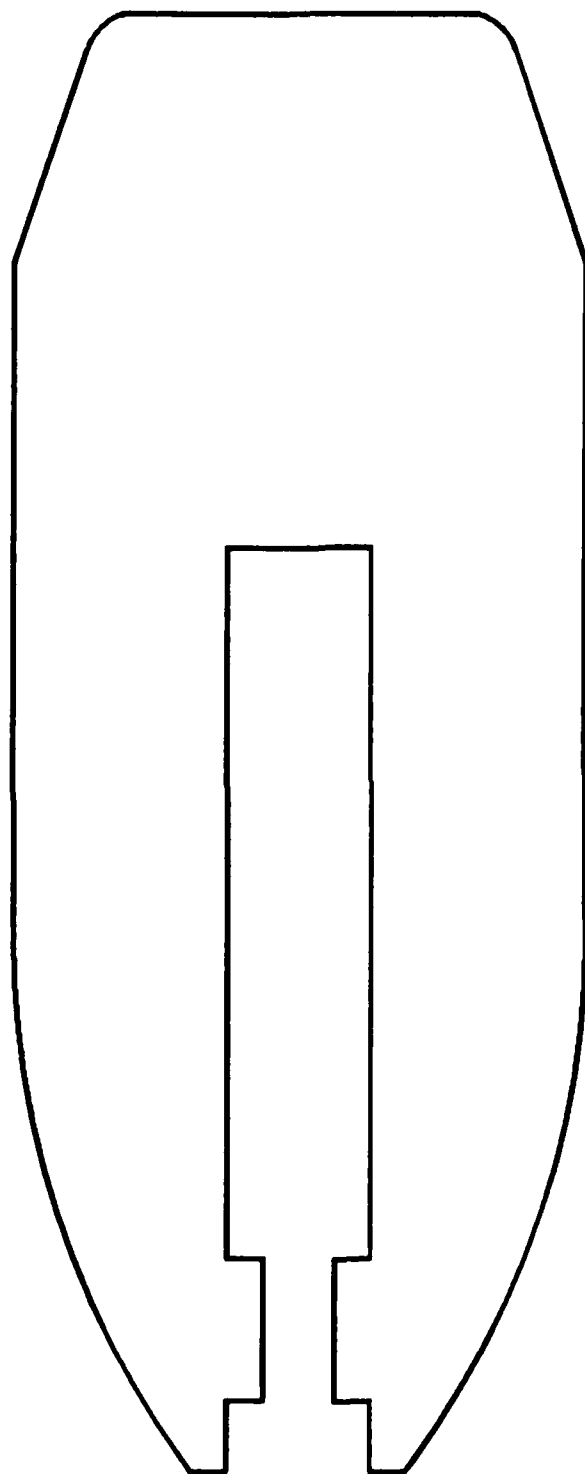
8

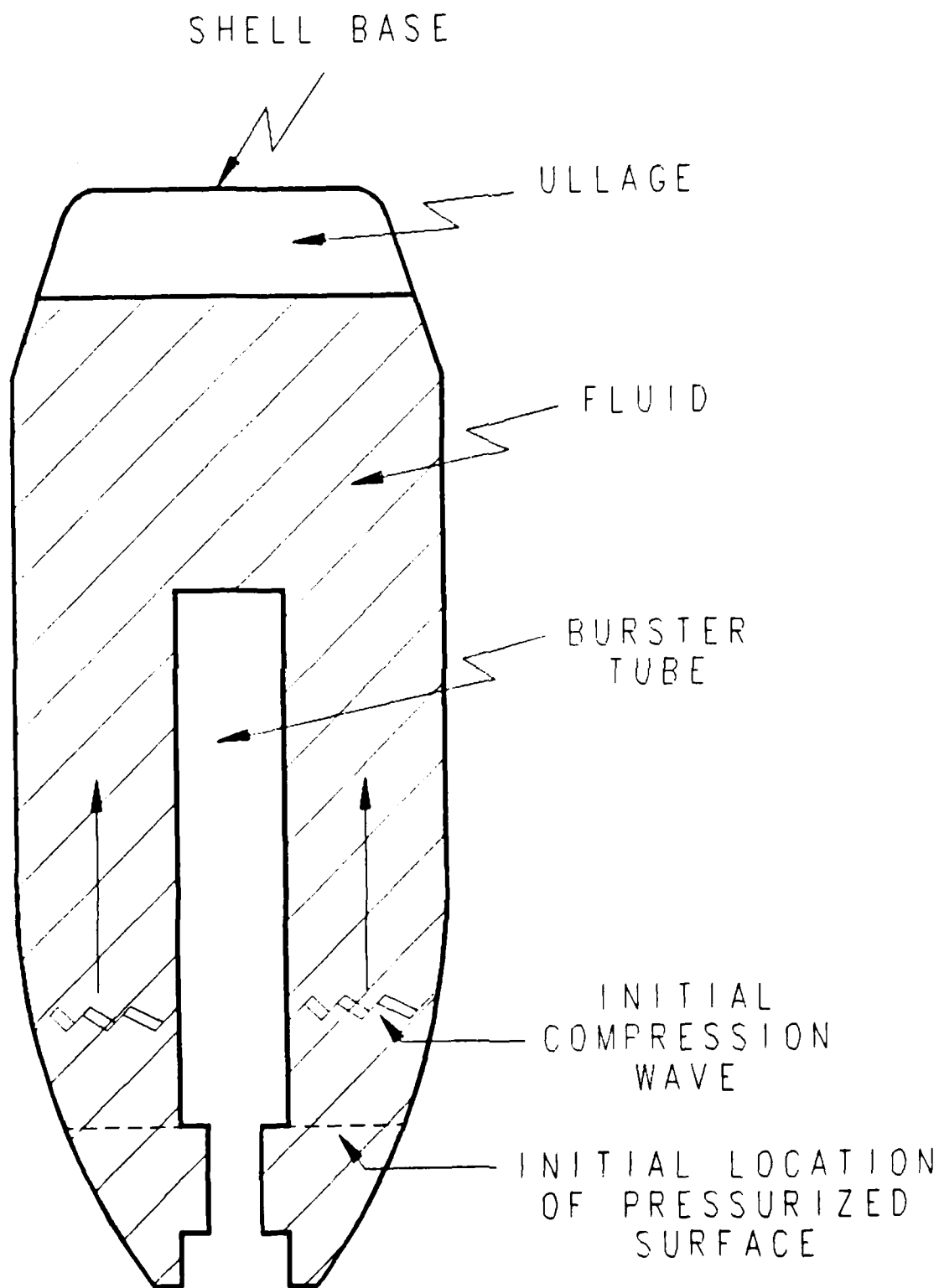Figure 1. Shell internal configuration.
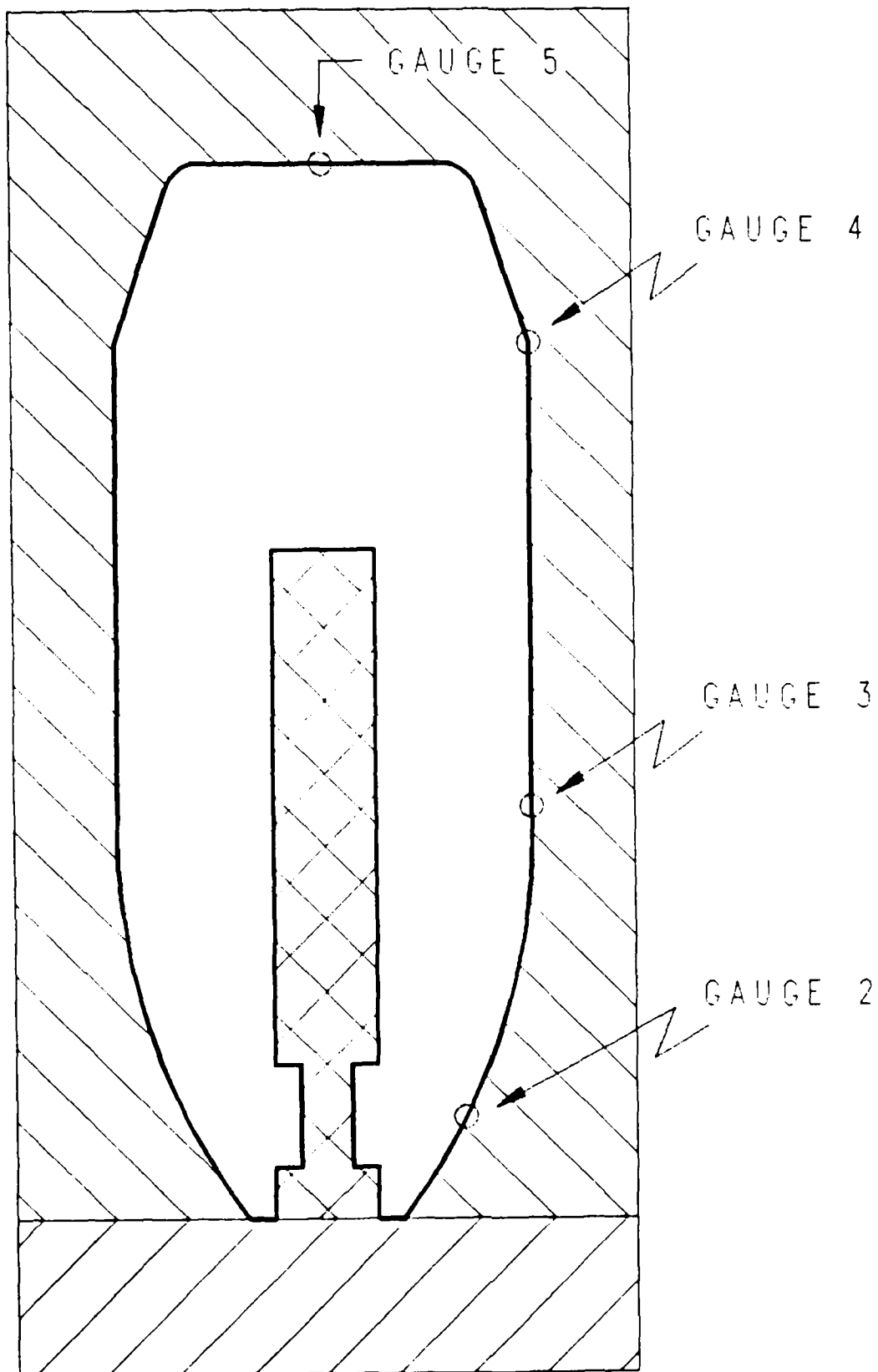
Figure 2. Motion of initial compression wave.

10

Figure 3. Experimental pressure gauge locations.
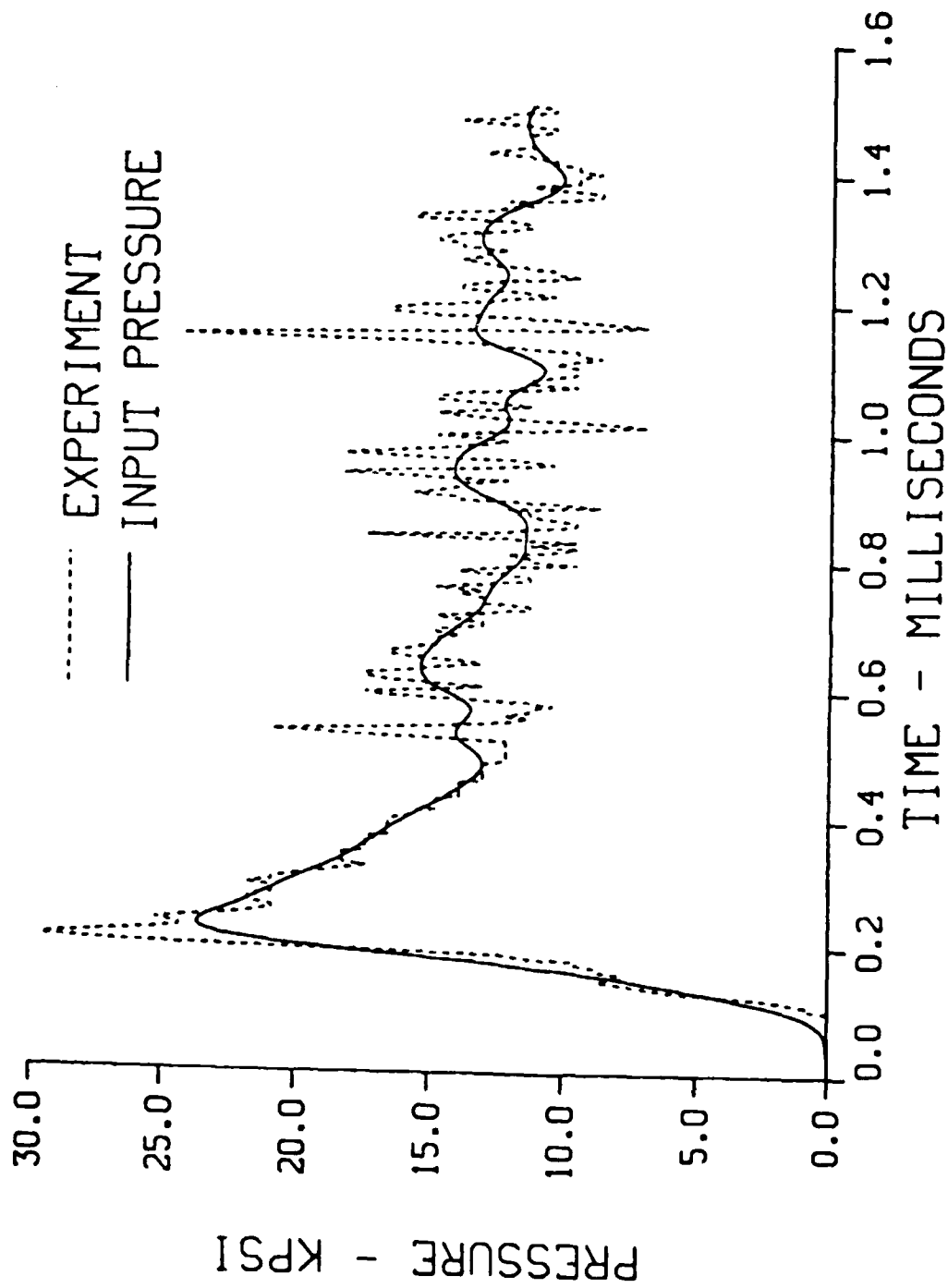
GAUGE 5

GAUGE 4

GAUGE 3

GAUGE 2

Figure 4a. Measured and smoothed data used as input pressure history at gauge 2, 40gm burster, 3" ullage.
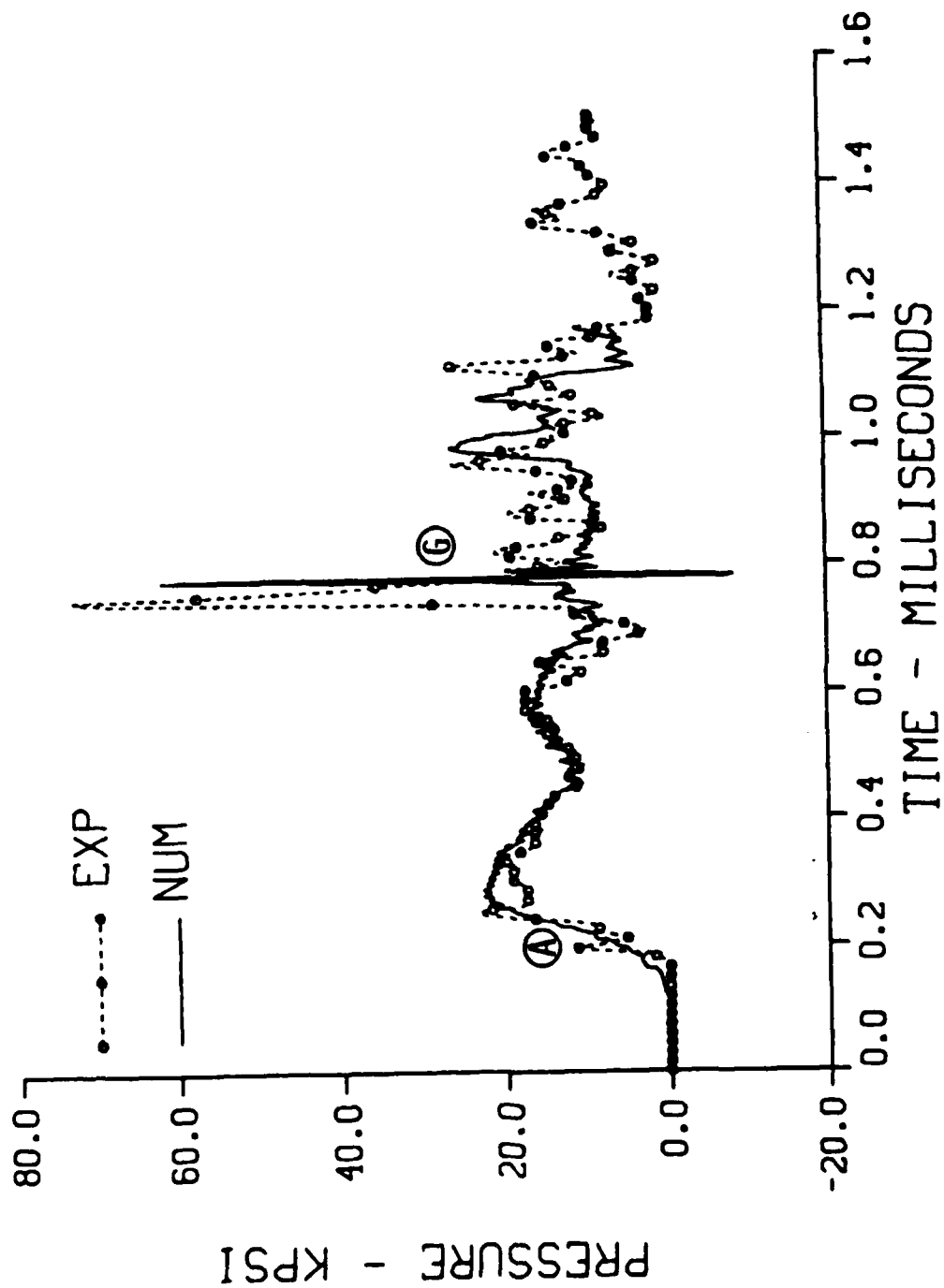
Figure 4b. Measured and computed pressure history at gauge 3, 40gm burster, 3% ullage.
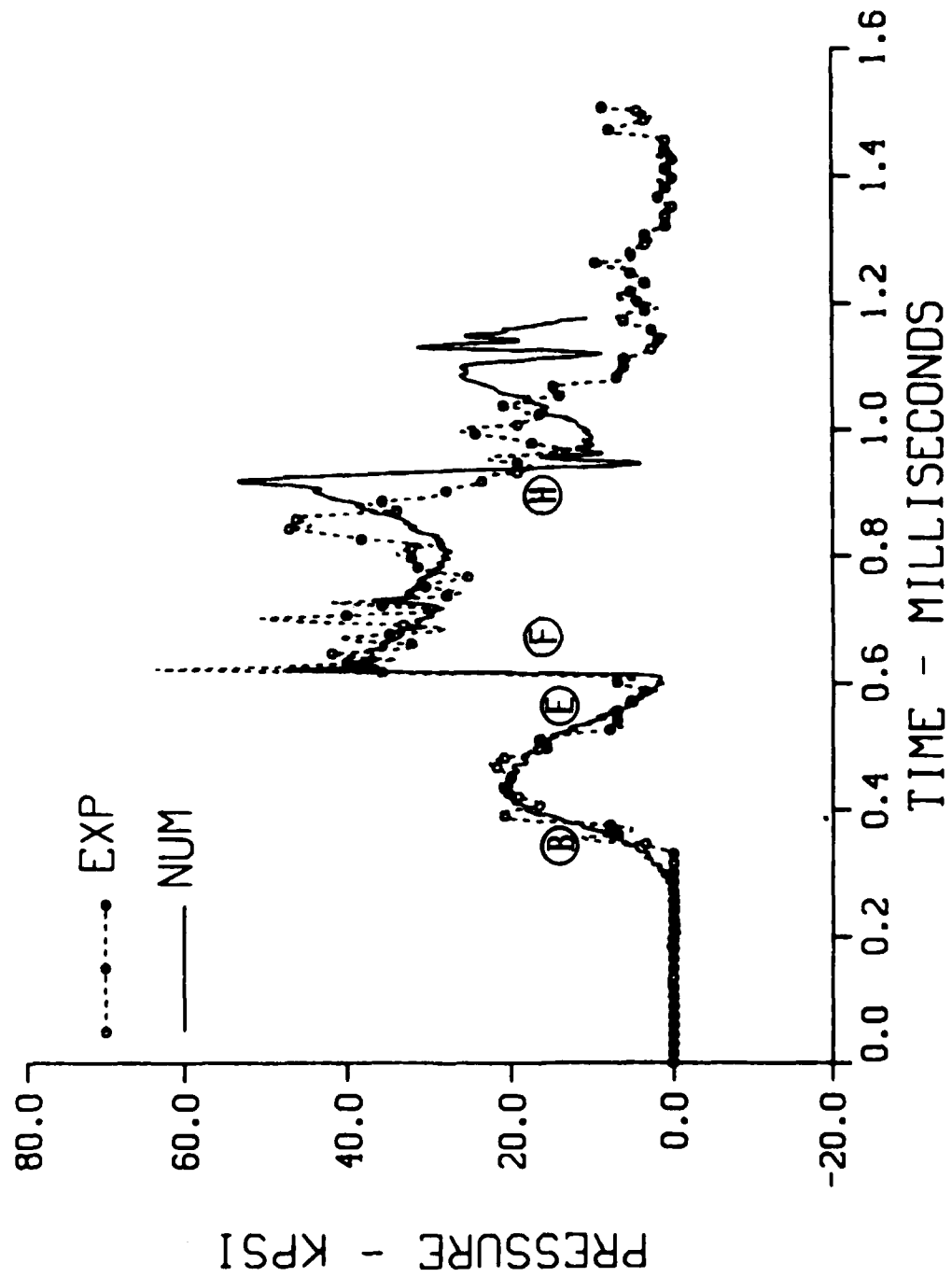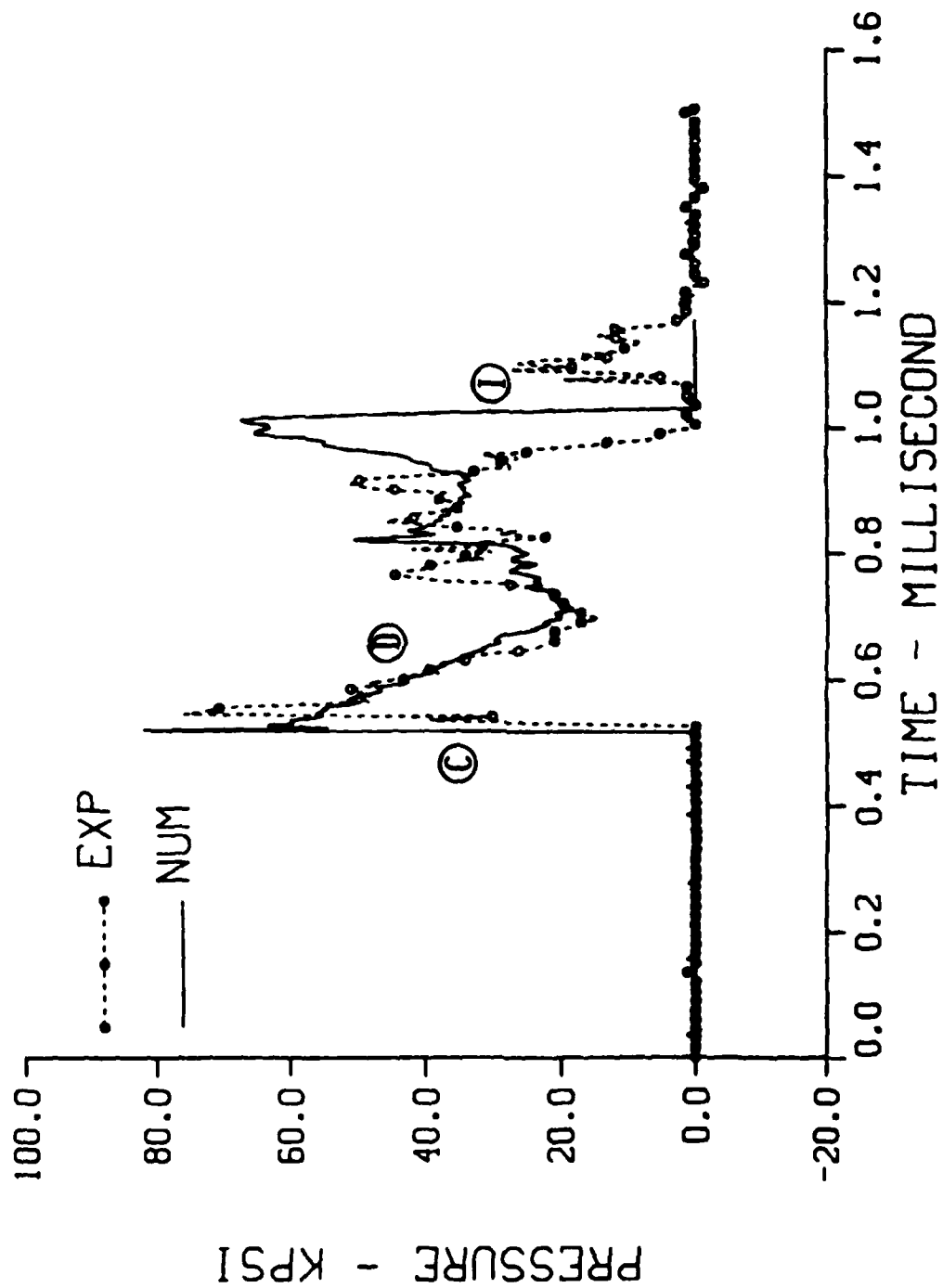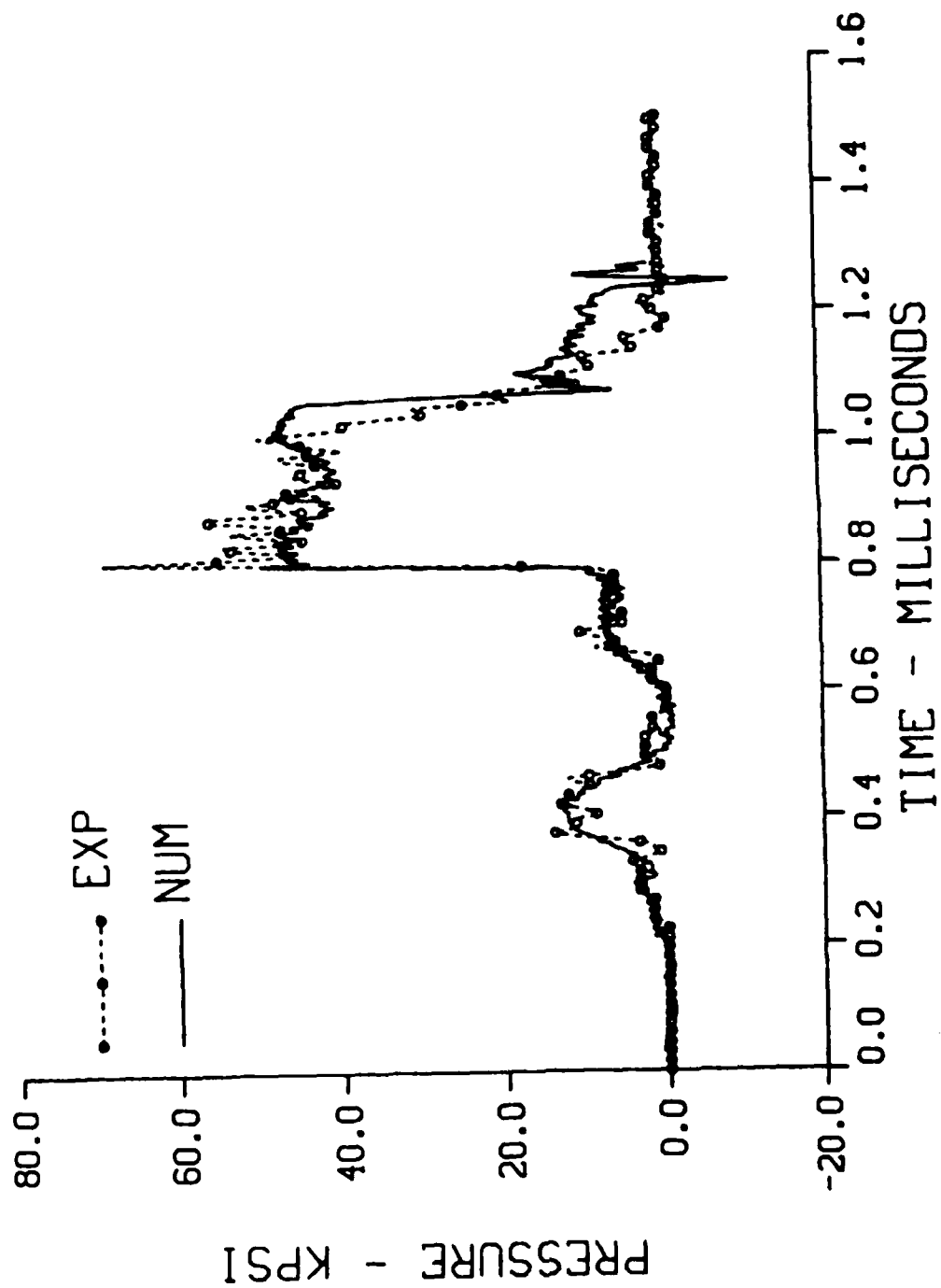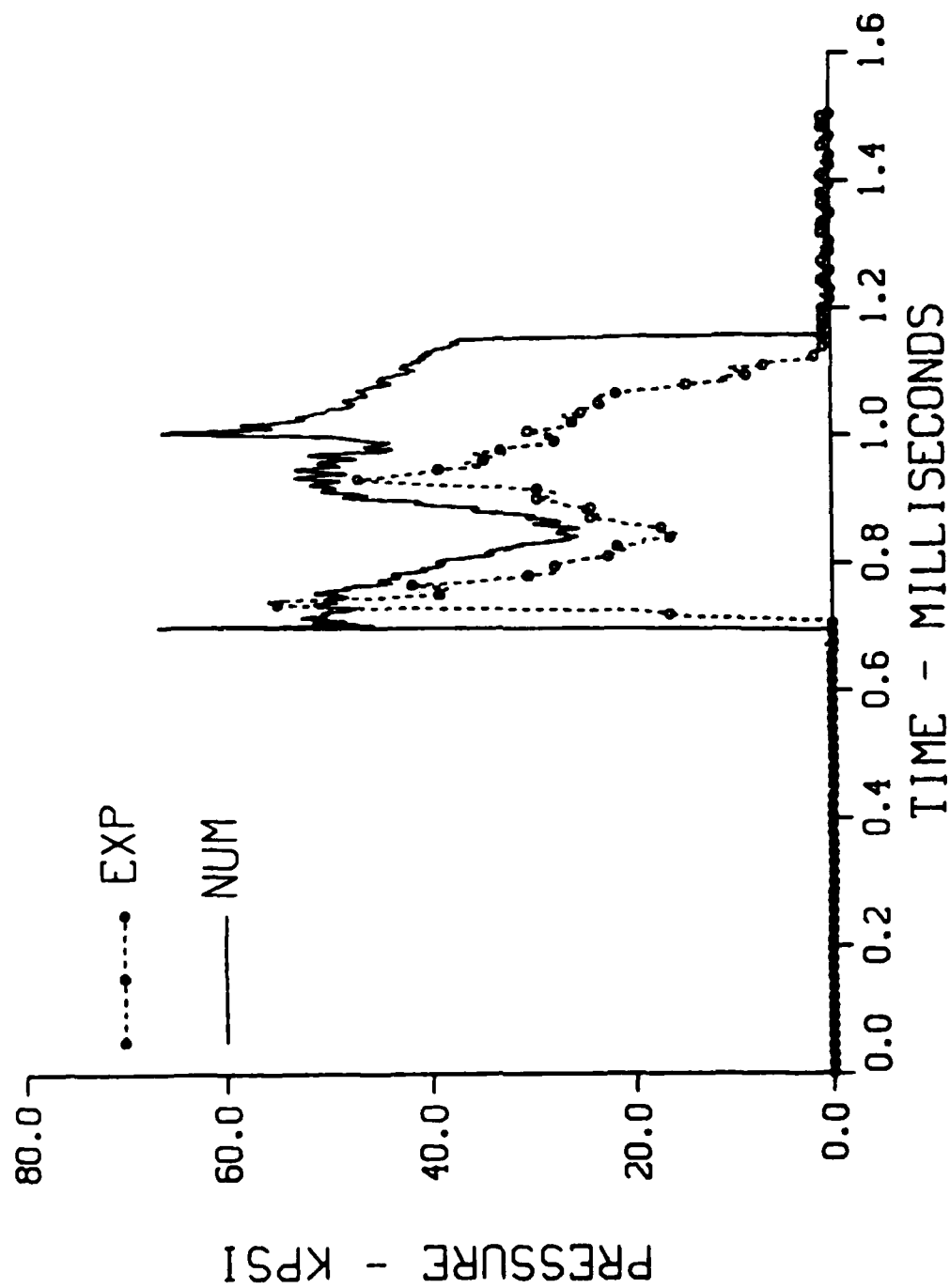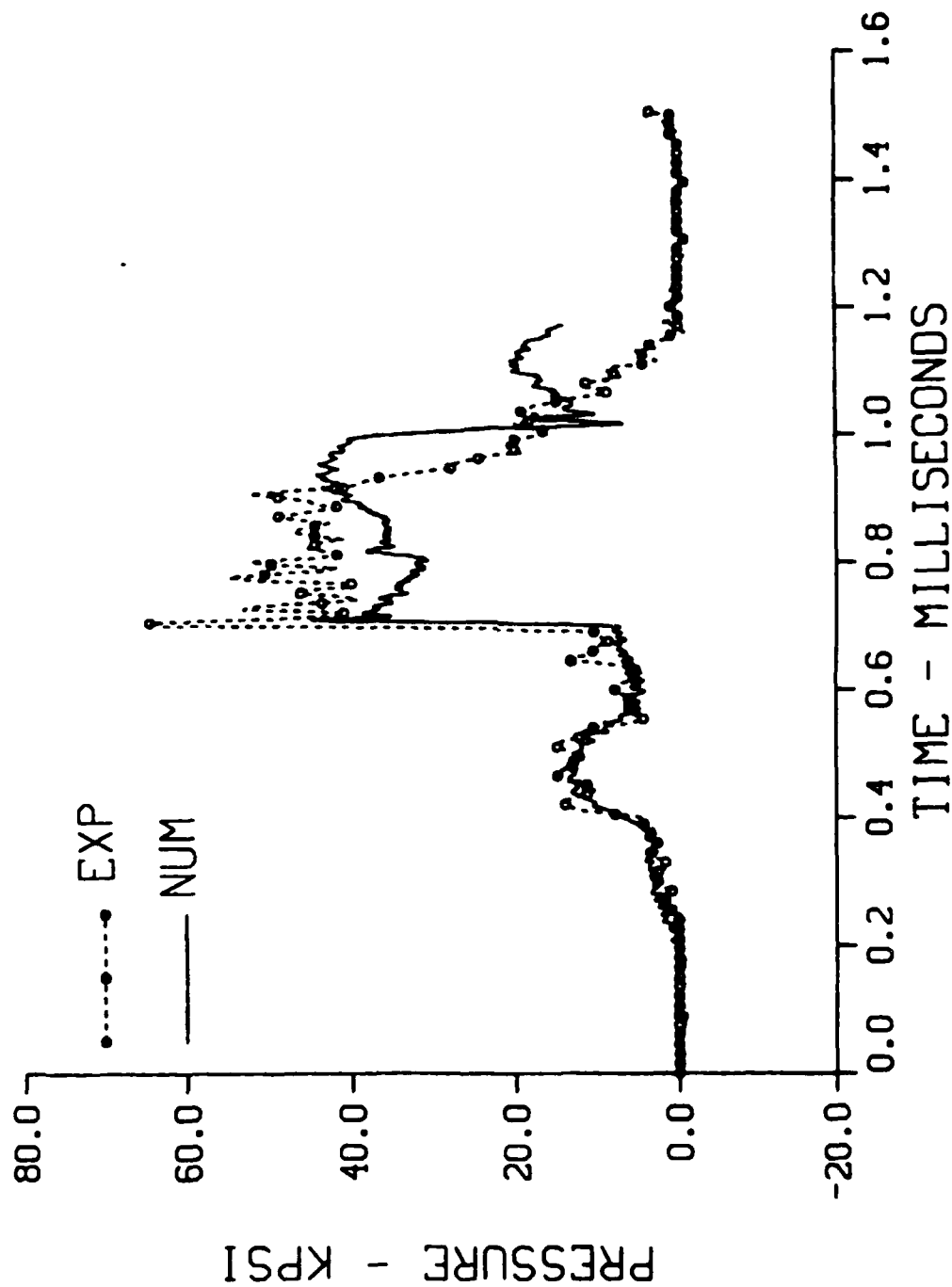
13

Figure 4c. Measured and computed pressure history at gauge 4, 40gm burster, 3% ullage.

14

Figure 4d. Measured and computed pressure history at gauge 5, 40gm burster, 3% ullage.

15

Figure 5a. Measured and computed pressure history at gauge 4, 40gm burster, 10% ullage.
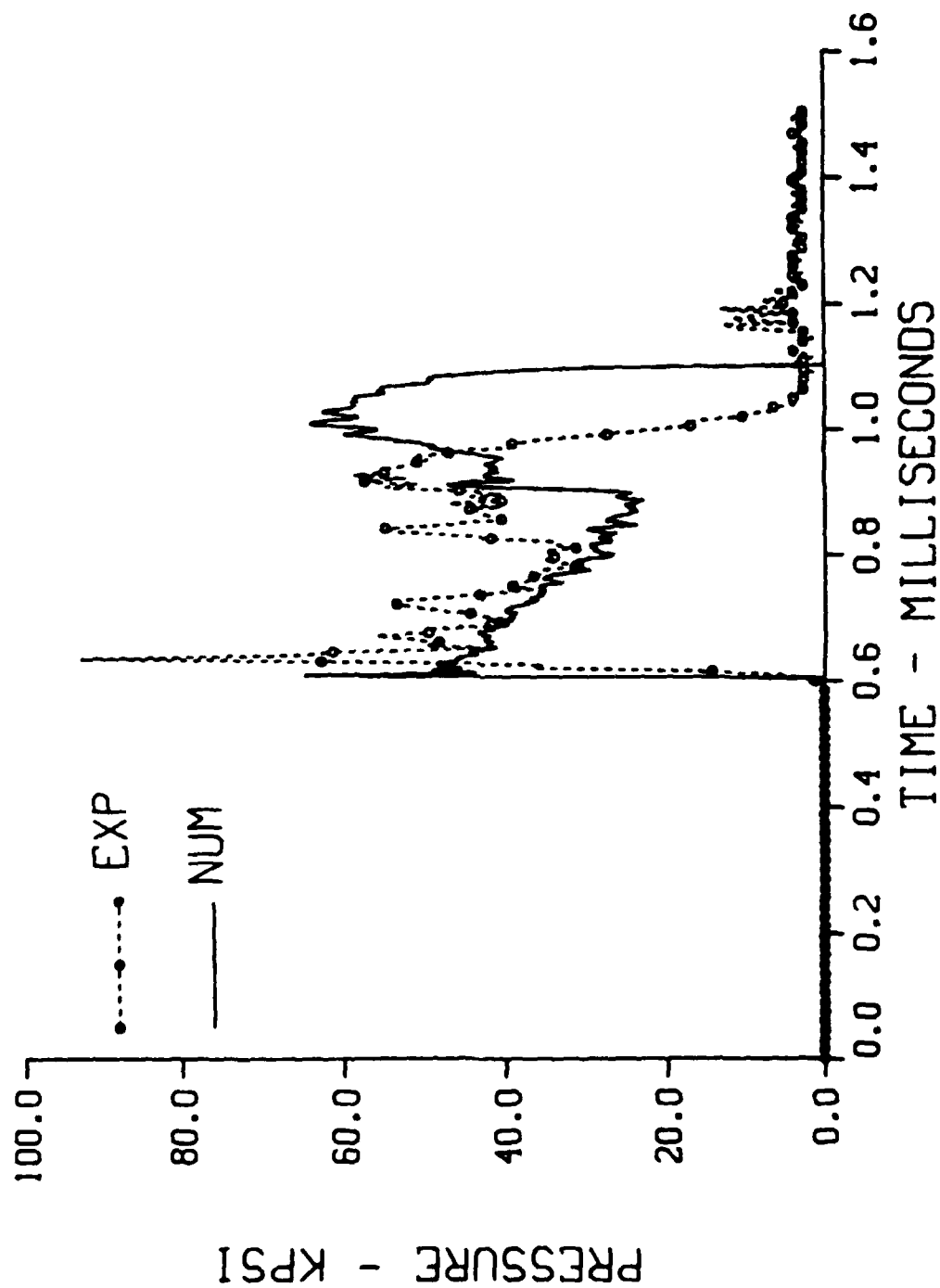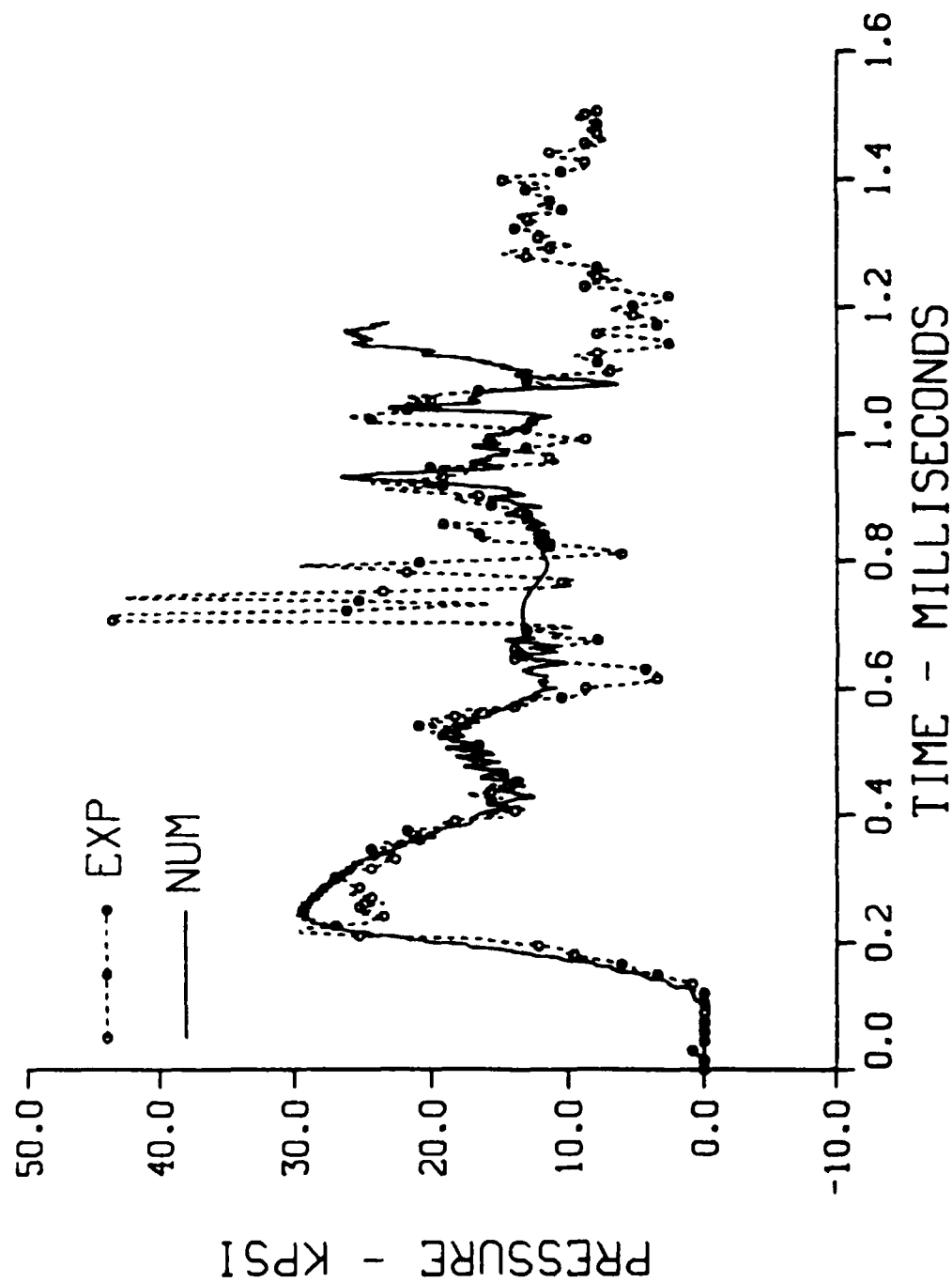
16

Figure 5b. Measured and computed pressure history at gauge 5, 40gm burster, 10% ullage.

17

Figure 6a. Measured and computed pressure history at gauge 4, 40gm burster, 5% ullage.

18

Figure 6b. Measured and computed pressure history at gauge 5, 40gm burster, 5% ullage.

19

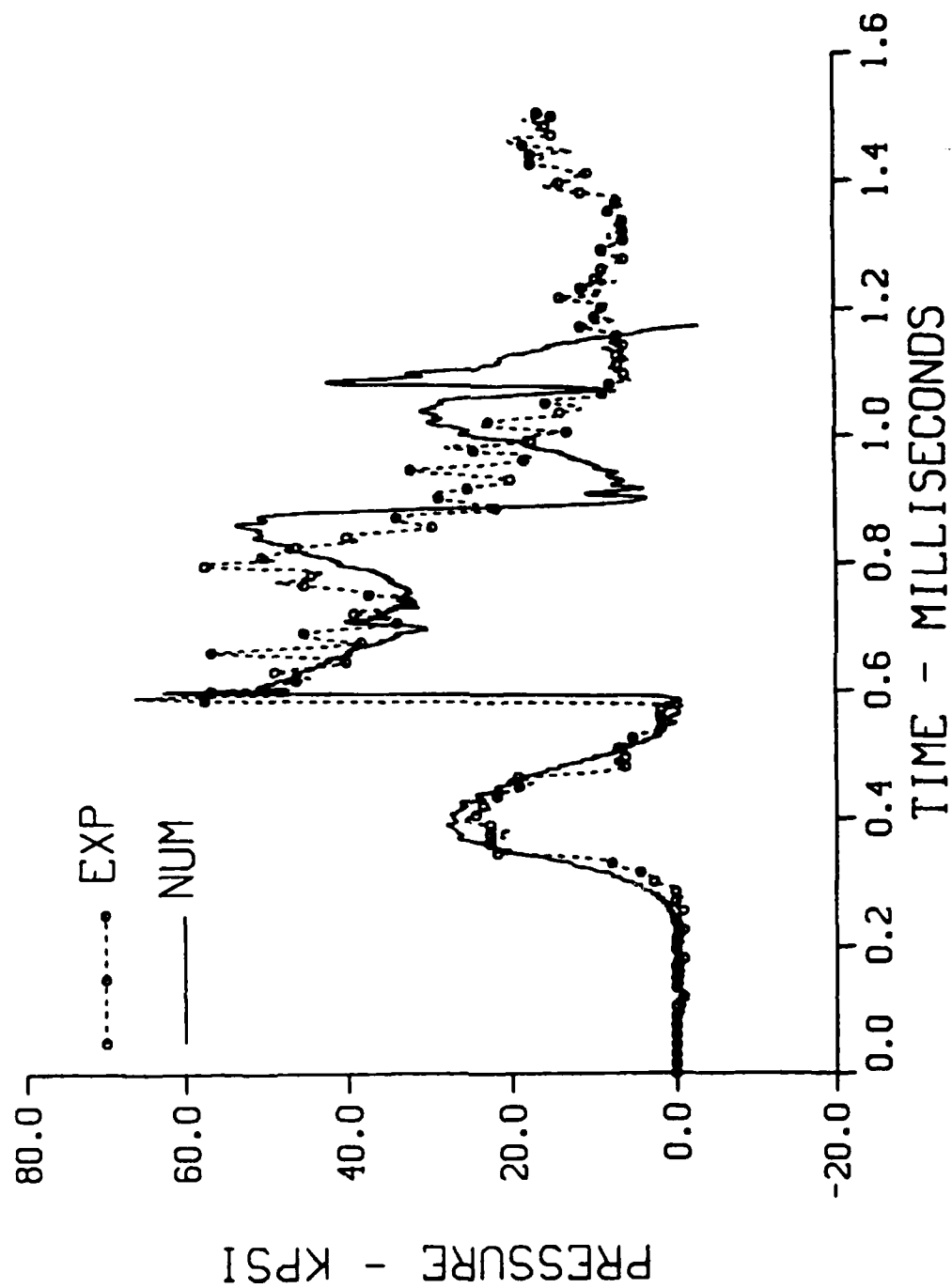Figure 7a. Measured and computed pressure history at gauge 3, 50gm burster, 5% ullage.

20

Figure 7h. Measured and computed pressure history at gauge 4, 50gm burster, 5% ullage.
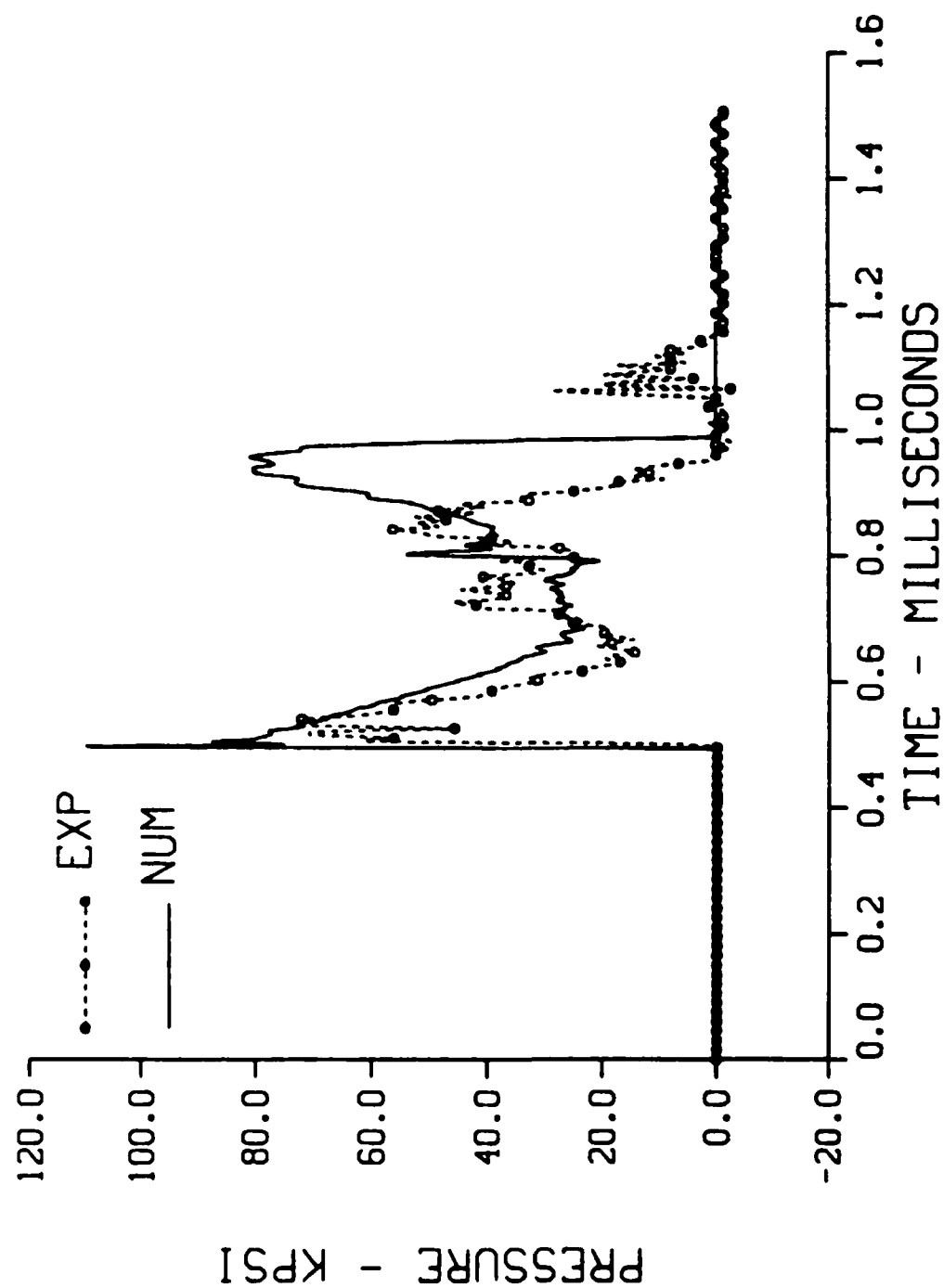
21

Figure 7c. Measured and computed pressure history at gauge 5, 50gm burster, 5% ullage.
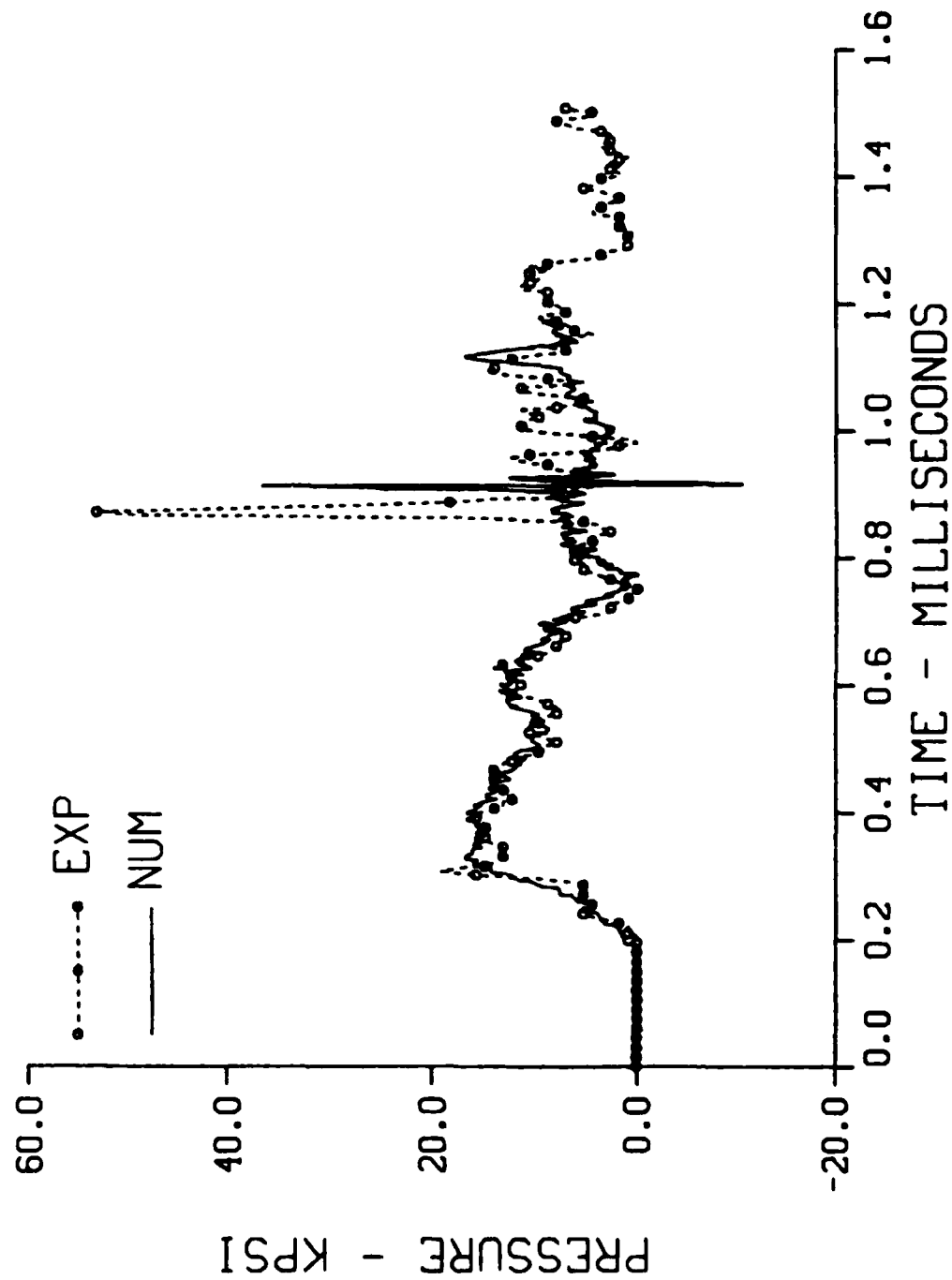
Figure 8a. Measured and computed pressure history at gauge 3, 30gm burster, 5% ullage.
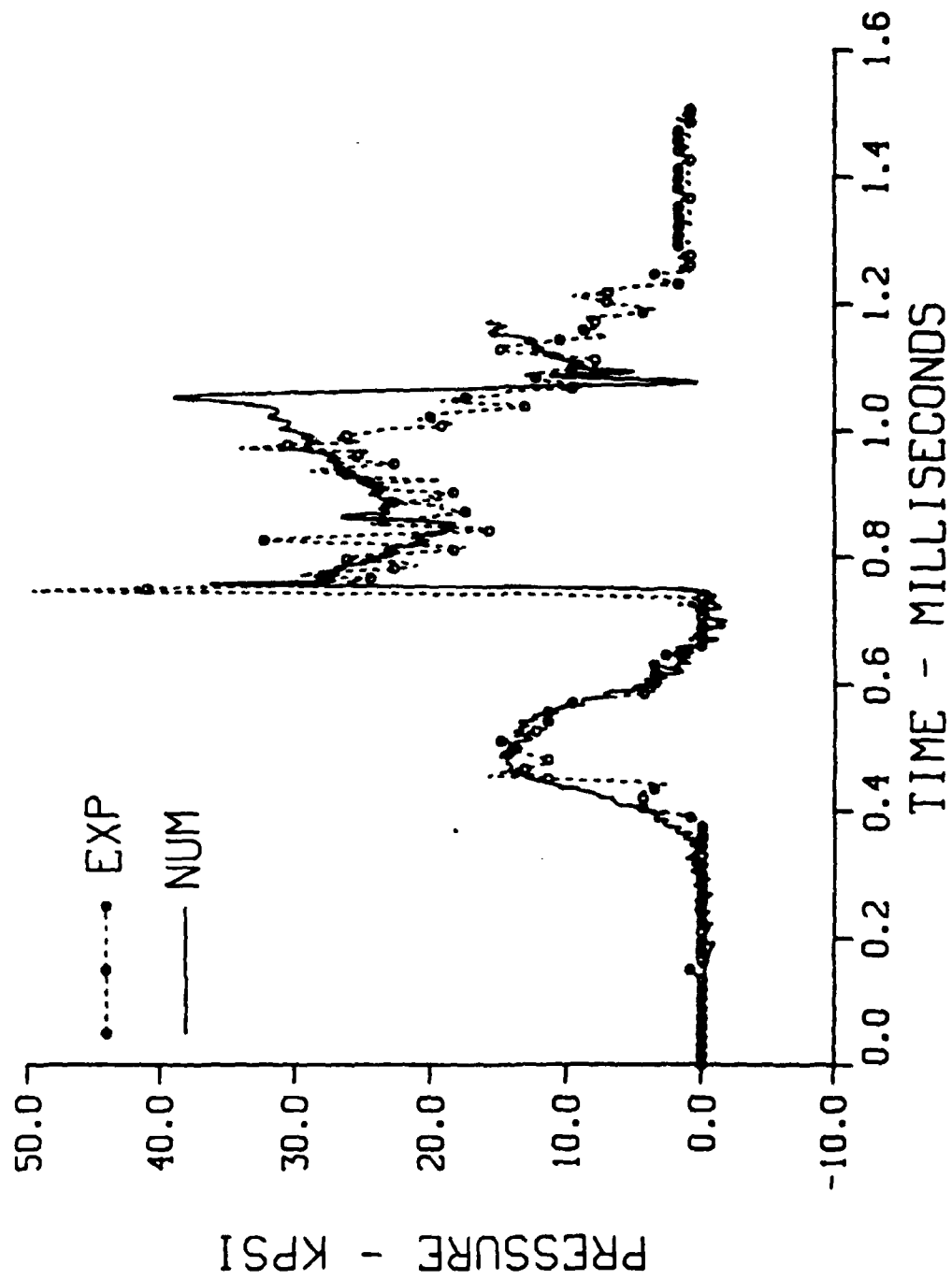
23

Figure 8b. Measured and computed pressure history at gauge 4, 30gm burster, 5% ullage.
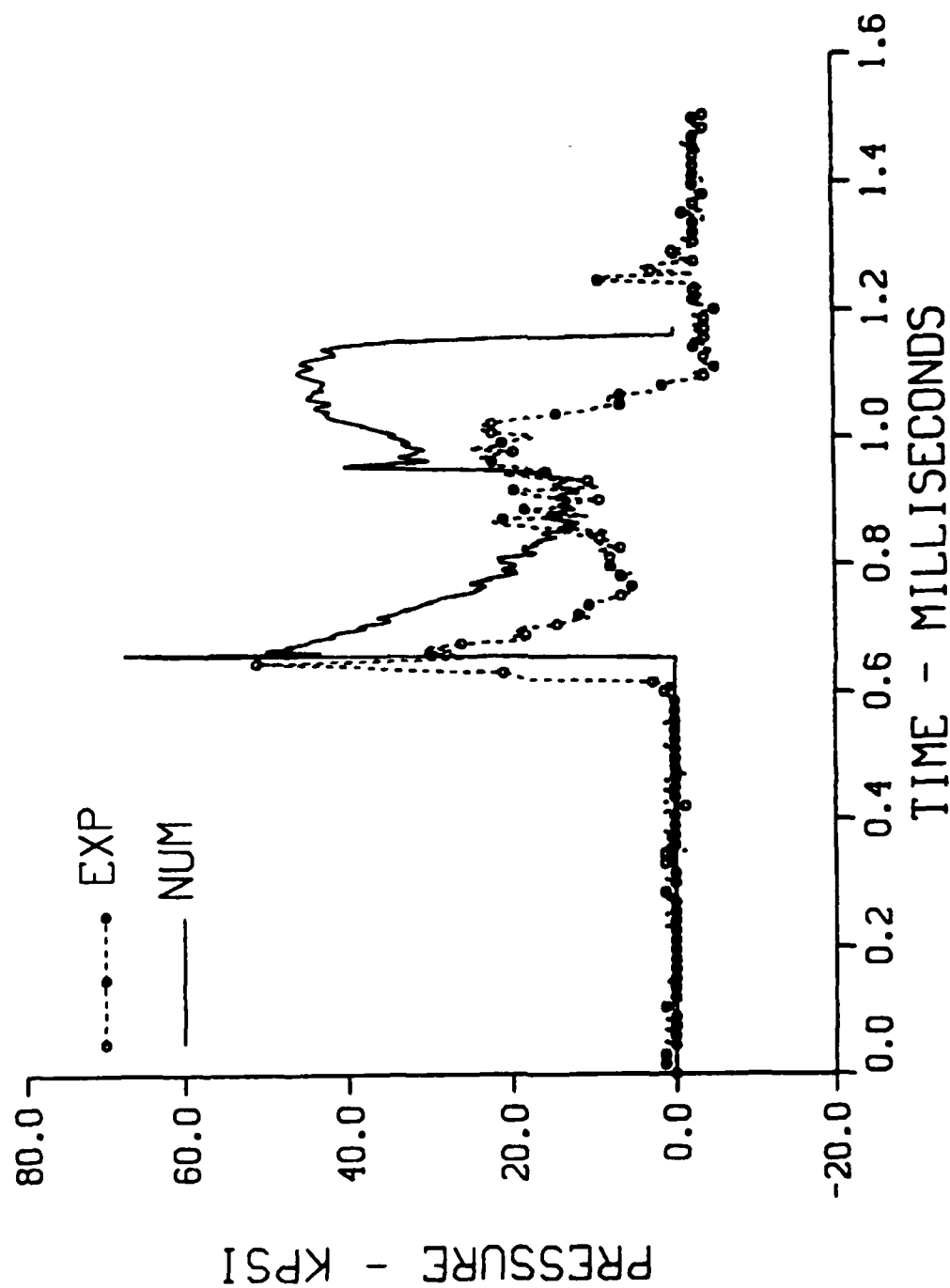
24

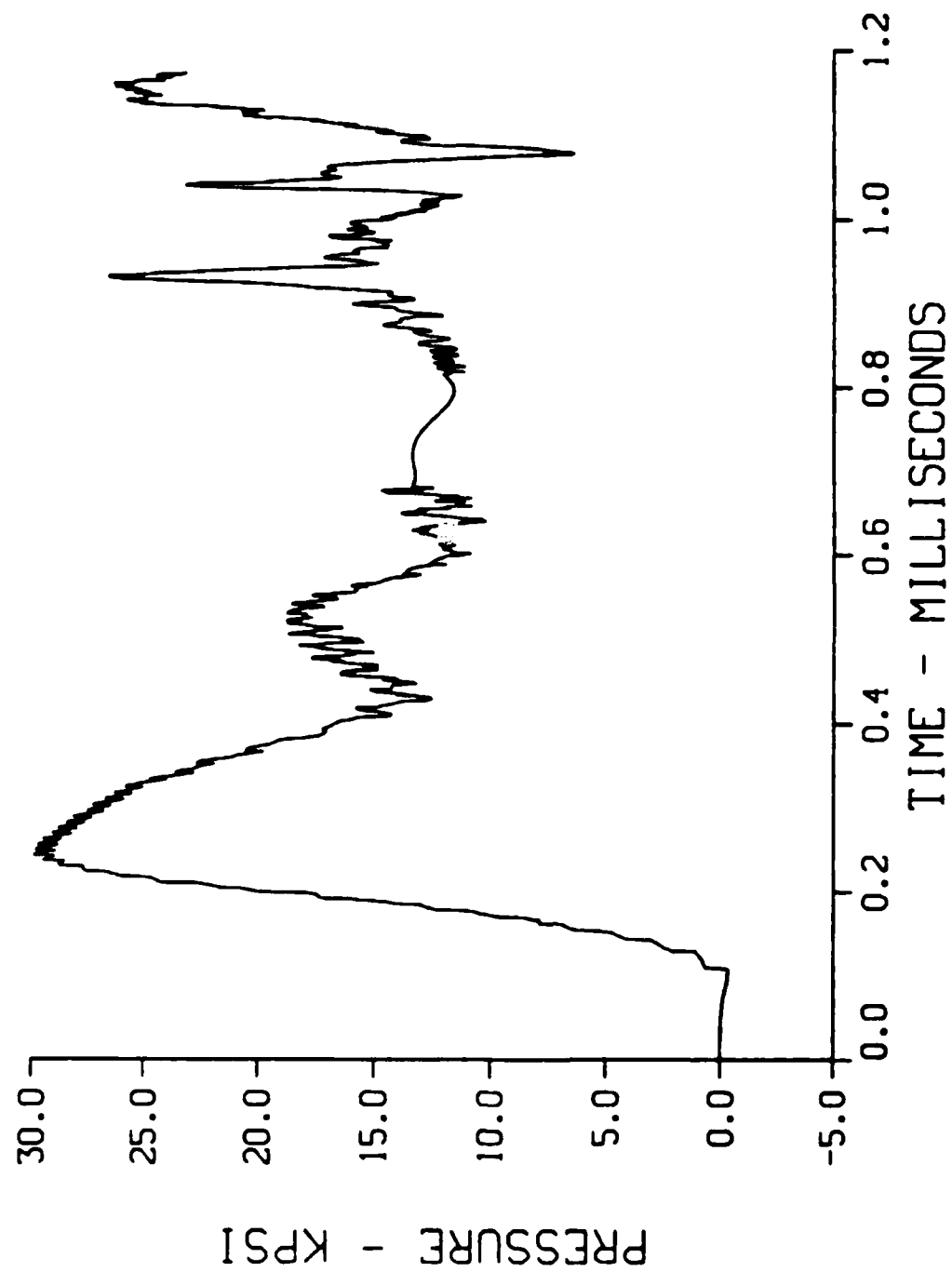Figure 8c. Measured and computed pressure history at gauge 5, 30gm burster, 5% ullage.

Figure 9a. Computed pressure history at gauge 3, 5% ullage, FF5 input pressure.
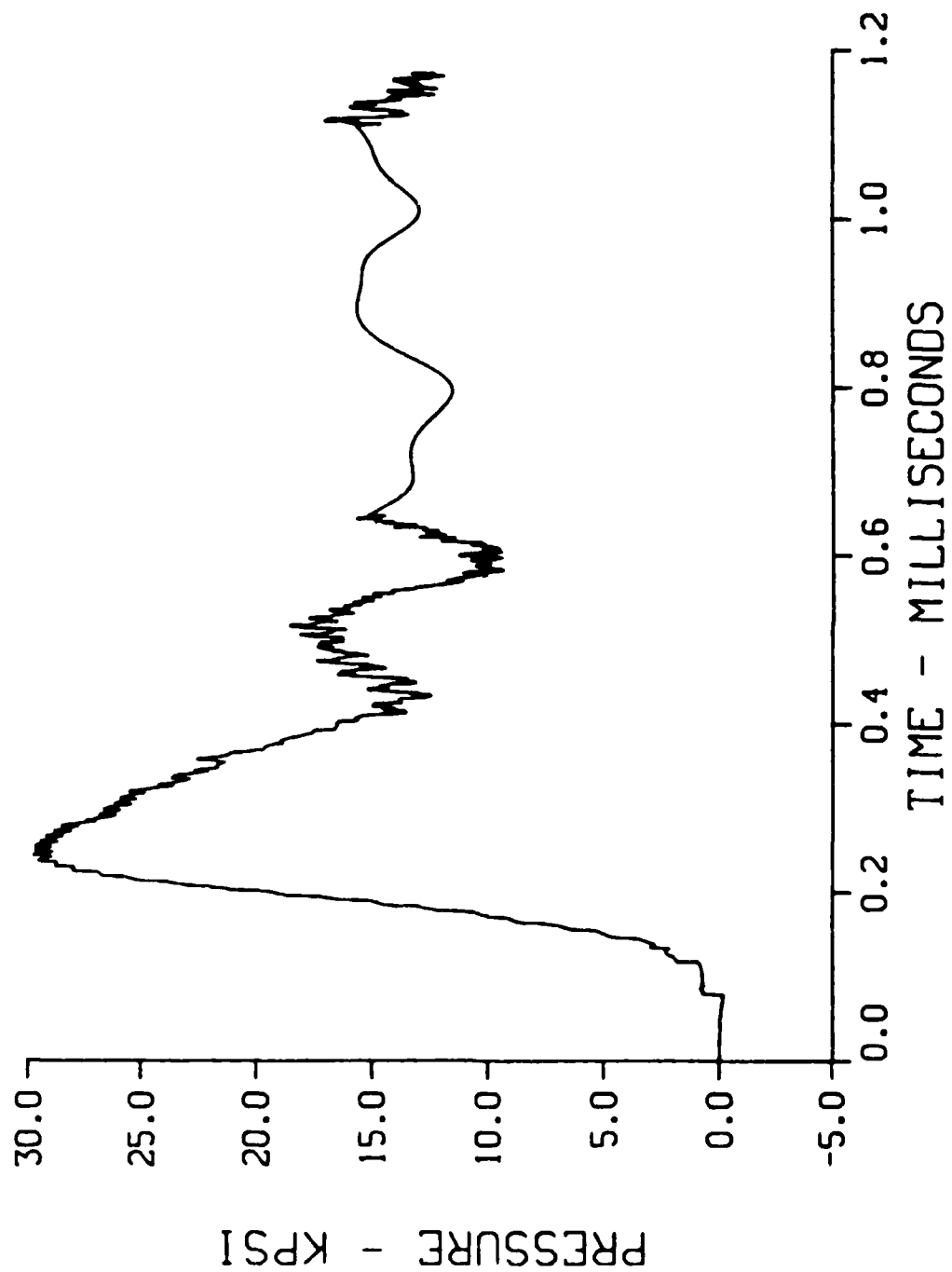
Figure 9b.   Computed pressure history at gauge 3, 10% ullage, FF5 input pressure.
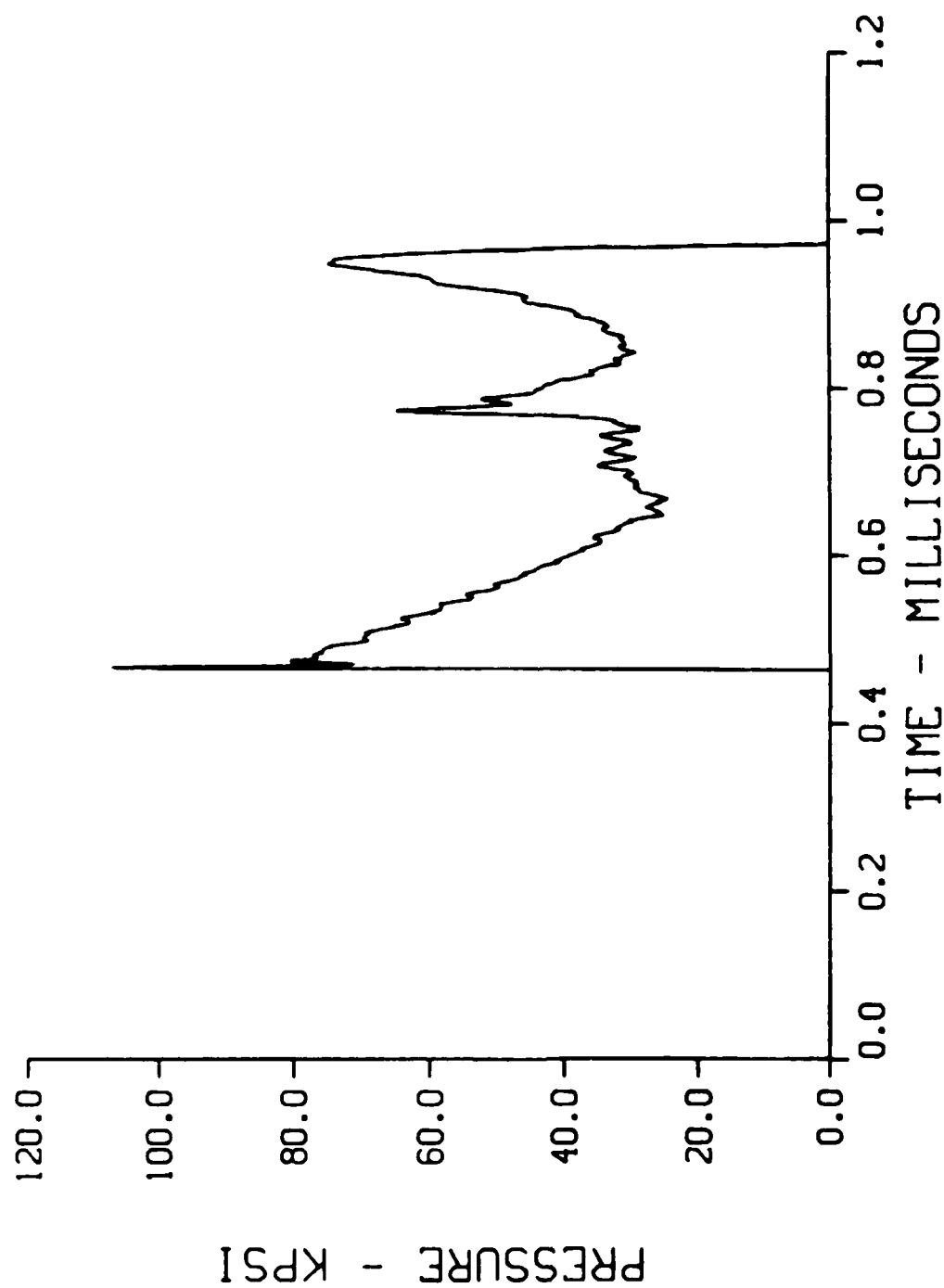
27

Figure 10a. Computed pressure history at gauge 5, 3% ullage, FF5 input pressure.

Figure 10b. Computed pressure history at gauge 5, 5% ullage, FF5 input pressure.

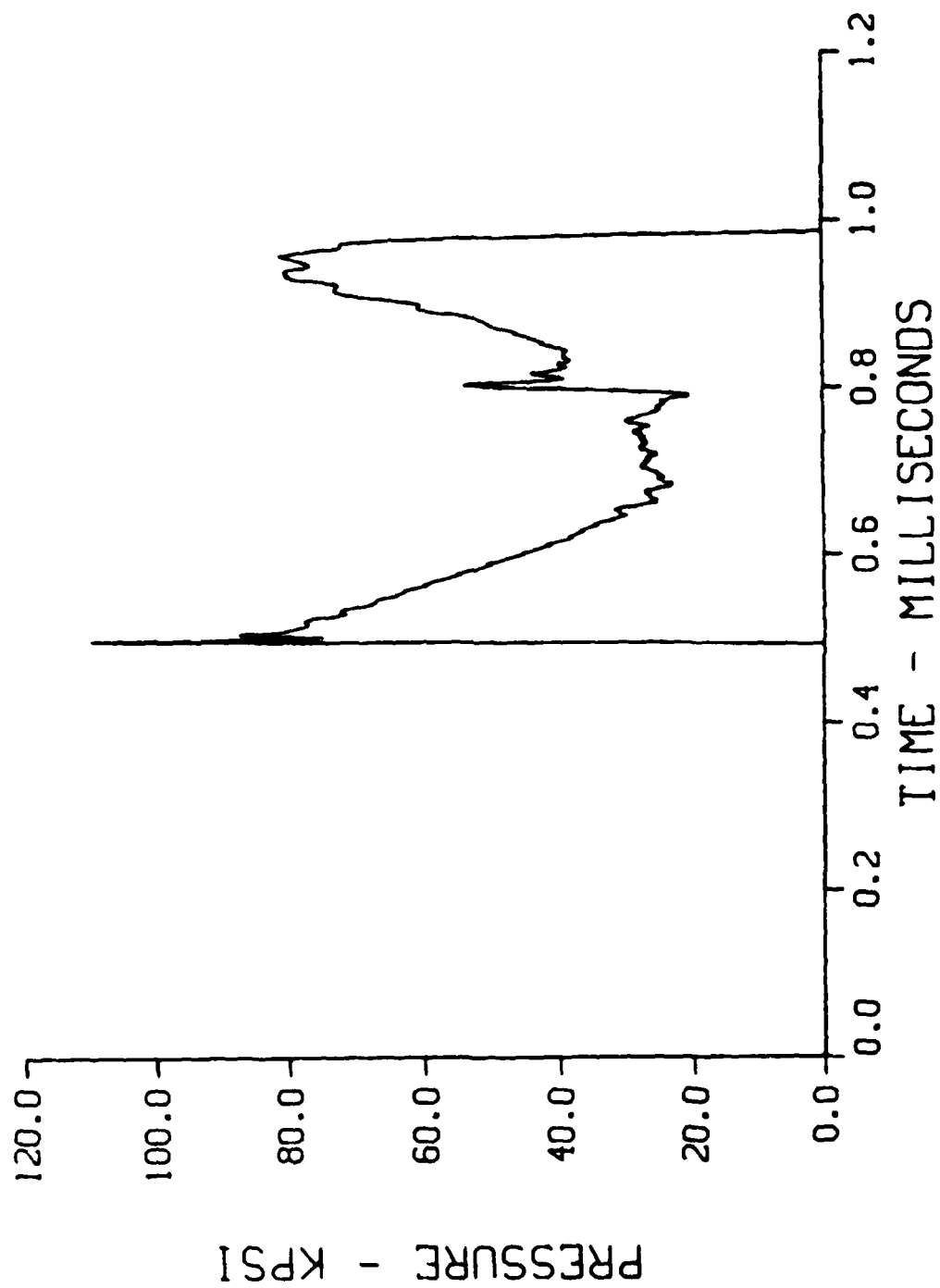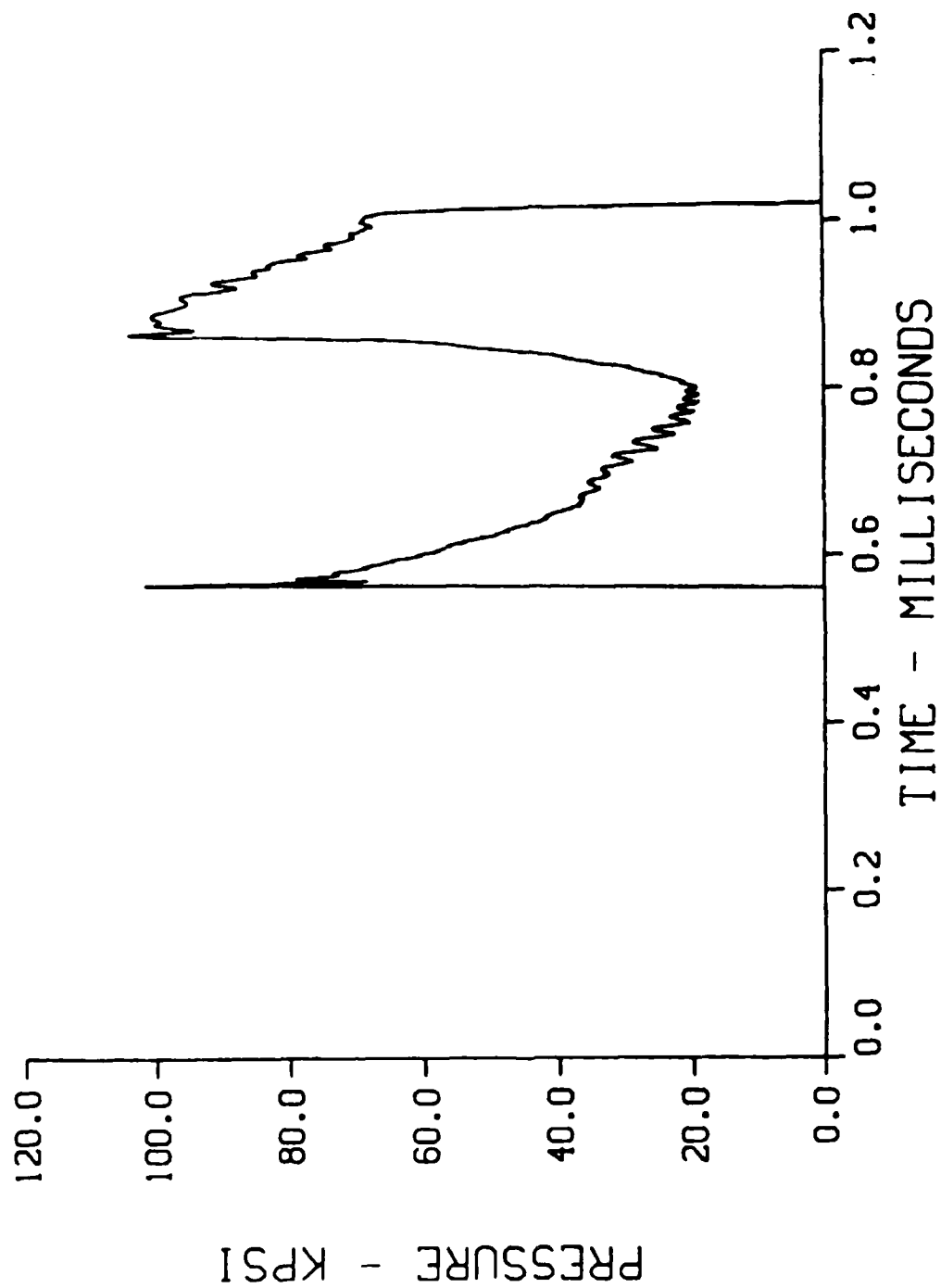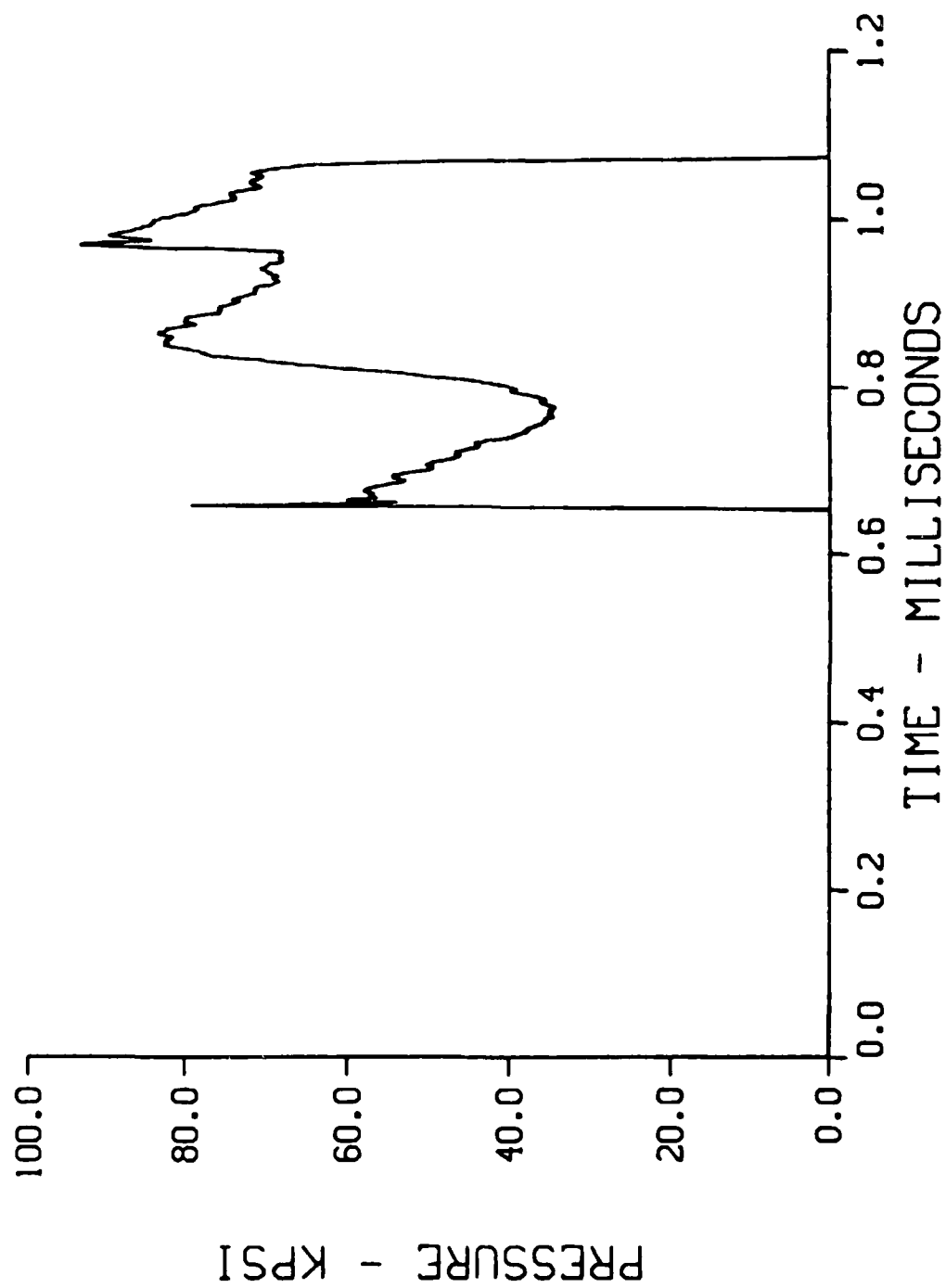Figure 10c. Computed pressure history at gauge 5, 10% ullage, FF5 input pressure.

30

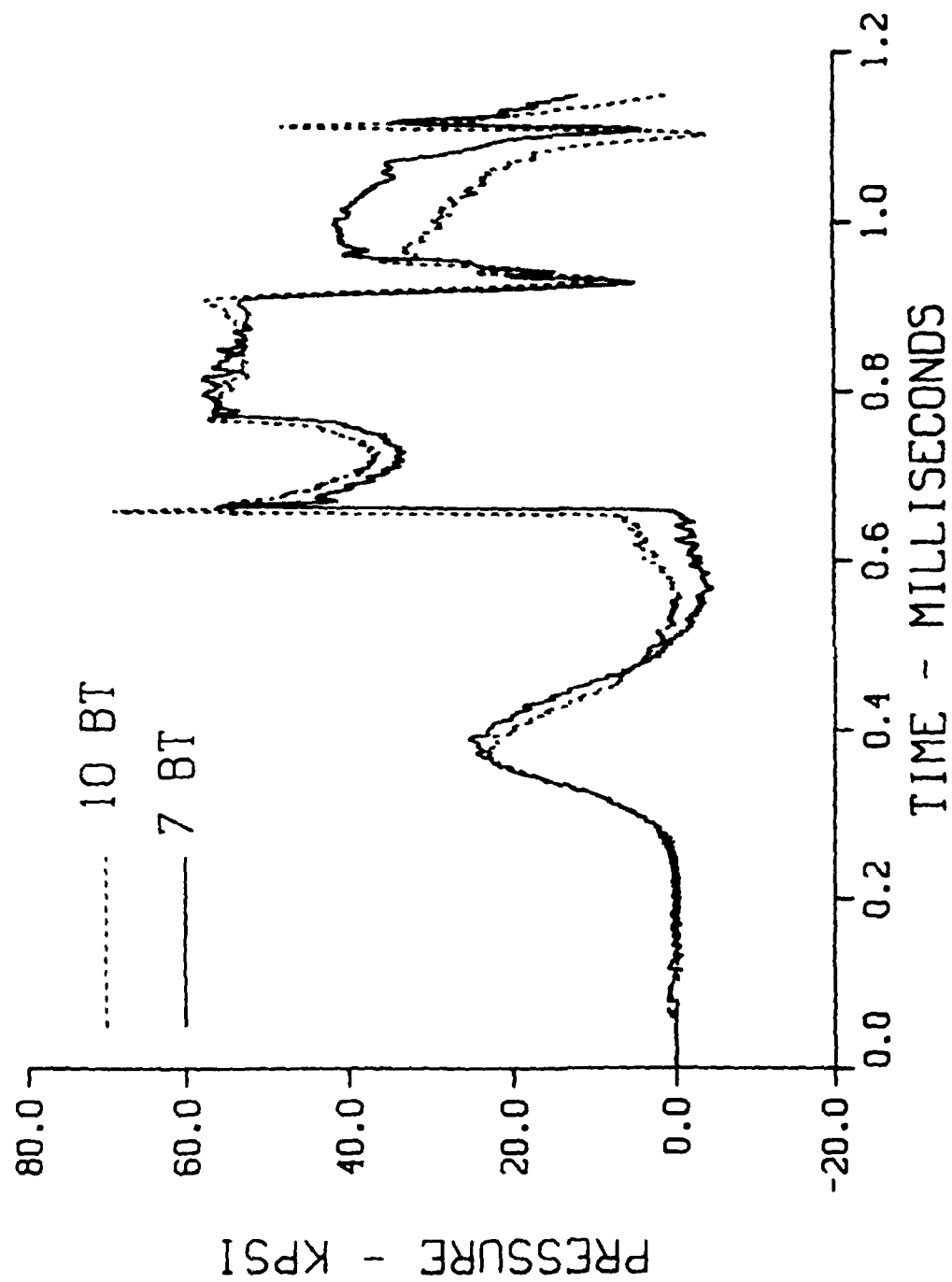Figure 10d. Computed pressure history at gauge 5, 15% ullage, FF5 input pressure.

31

Figure 11a. Computed pressure history at gauge 4, 10% ullage, 7 and 10 degree internal boattail angle, FF5 input pressure.

32

Figure 11b. Computed pressure history at gauge 5, 10% ullage, 7 and 10 degree internal boattail angle, FF5 input pressure.

33

REFERENCES

1. Weinacht, P. and Nietubicz, C.J., "Wave Motion Analysis of a Nonspinning Liquid Filled Cylinder," ARBRL-MR-3451, U.S. Army Ballistics Research Laboratory, Aberdeen Proving Ground, Maryland, June 1985.

2. Watson, J.L., private communications concerning unpublished test data, Project Officer, U.S. Army Ballistic Research Laboratory, Aberdeen Proving Ground, Maryland, February 1986.

3. Roberson, J.A. and Crowe, C.T., "Engineering Fluid Mechanics," Houghton Mufflin Company, Boston, c 1975

4. Carmichael, C., "Kent's Mechanical Engineers' Handbook, Design and Production," Twelfth Edition, Wiley Handbook Series, 1964.

5. Anderson, D.A., Tannehill, J.C., and Pletcher, R.H., "Computational Fluid Mechanics and Heat Transfer," McGraw-Hill Book Company, New York, c 1984

LIST OF SYMBOLS

A   =   local cross sectional area

E   =   fluid bulk modulus

F   =   flux vector

F   =   flux vector normalized by Jacobian

H   =   source term due to area change

H   =   source term normalized by Jacobian

J   =   Jacobian of the transformation

P   =   pressure

q   =   vector of dependent variables

q   =   vector of dependent variables scaled by Jacobian

t   =   time

u   =   axial velocity

x   =   axial coordinate

ρ =   density

ρ_0 =   density at ambient conditions

Subscripts

t   =   derivative with respect to time

x   =   derivative with respect to axial coordinate

ξ =   derivative with respect to spacial computational coordinate

Superscripts

N   =   denotes solution at "N"th time level

N+1   =   denotes solution at "N+1"th time level

$\overline{N+1}$ =   denotes solution at end of "N+1"th predictor step

DISTRIBUTION LIST

No. of Copies	Organization	No. of Copies	Organization

12 Administrator
  Defense Technical Info Center
  ATTN: DTIC-FDAC
  Cameron Station, Bldg. 5
  Alexandria, VA 22304-6145

1 HQDA
  DAMA-ART-M
  Washington, DC 20310

1 Commander
  US Army Materiel Command
  ATTN: AMCDRA-ST
  5001 Eisenhower Avenue
  Alexandria, VA 22333-0001

8 Commander
  US Army Armament Research,
    Development and Engineering
    Center
  ATTN: SMCAR-MSI
        SMCAR-LCA-F/Kline
                    Fleming
                    Kahn
                    Hudgins
        SMCAR-CCL-CA/Hirlinger
                    O'Niell
                    Miller
  Dover, NJ 07801-5001

1 Commander
  US Army Armament Research,
    Development and Engineering
    Center
  ATTN: SMCAR-TDC
  Dover, NJ 07801-5001

1 Commander
  US AMCCOM ARDEC CCAC
  Benet Weapons Laboratory
  ATTN: SMCAR-CCB-TL
  Watervliet, NY 12189-4050

1 Commander
  US Army Armament, Munitions and
    Chemical Command
  ATTN: AMSMC-IMP-L
  Rock Island, IL 61299-7300

1 Commander
  US Army Aviation Systems Command
  ATTN: AMSAV-ES
  4300 Goodfellow Blvd
  St. Louis, MO 63120-1798

1 Director
  US Army Aviation Research and
    Technology Activity
  Ames Research Center
  Moffett Field, CA 94035-1099

10 C.I.A.
  OIR/DB/Standard
  GE47 HQ
  Washington, DC 20505

1 Commander
  US Army Communications -
    Electronics Command
  ATTN: AMSEL-ED
  Fort Monmouth, NJ 07703-5301

1 Commander
  CECOM R&D Technical Library
  ATTN: AMSEL-IM-L
        (Reports Section) B.2700
  Fort Monmouth, NJ 07703-5000

3 Commander
  US Army Missile Command
    Research, Development and
    Engineering Center
  ATTN: AMSMI-RD
  Redstone Arsenal, AL 35898-5230

1 Director
' US Army Missile and Space
    Intelligence Center
  ATTN: AIAMS-YDL
  Redstone Arsenal, AL 35898-5500

1 Commander
  US Army Tank Automotive Command
  ATTN: AMSTA-TSL
  Warren, MI 48397-5000

DISTRIBUTION LIST

No. of Copies	Organization	No. of Copies	Organization

1   Director
US Army TRADOC Analysis Center
ATTN: ATOR-TSL
White Sands Missile Range, NM
                  88002-5502

1   Commandant
US Army Infantry School
ATTN: ATSH-CD-CS-OR
Fort Benning, GA 31905-5400

1   Commander
US Army Development and
  Employment Agency
ATTN: MODE-ORO
Fort Lewis, WA 98433-5000

1   AFWL/SUL
Kirtland AFB, NM 87117

1   Air Force Armament Laboratory
ATTN: AFATL/DLODL
       (Tech Info Center)
Eglin AFB, FL 32542-5000

Aberdeen Proving Ground

Dir, USAMSAA
  ATTN: AMXSY-D
         AMXSY-MP, H. Cohen

Cdr, USATECOM
  ATTN: AMSTE-SI-F

Cdr, CRDC, AMCCOM,
    ATTN: SMCCR-RSP-A
          SMCCR-MU
          SMCCR-SPS-IL
          Mr. Henry Bach
          Mr. Ed Doyle

USER EVALUATION SHEET/CHANGE OF ADDRESS

This Laboratory undertakes a continuing effort to improve the quality of the reports it publishes. Your comments/answers to the items/questions below will aid us in our efforts.

1. BRL Report Number_____Date of Report_____

2. Date Report Received_____

3. Does this report satisfy a need? (Comment on purpose, related project, or other area of interest for which the report will be used.)_____

_____

_____

4. How specifically, is the report being used? (Information source, design data, procedure, source of ideas, etc.)_____

_____

_____

5. Has the information in this report led to any quantitative savings as far as man-hours or dollars saved, operating costs avoided or efficiencies achieved, etc? If so, please elaborate._____

_____

_____

6. General Comments. What do you think should be changed to improve future reports? (Indicate changes to organization, technical content, format, etc.)

_____

_____

_____

	_____
	Name
CURRENT ADDRESS	Organization
	_____
	Address
	City, State, Zip

7. If indicating a Change of Address or Address Correction, please provide the New or Correct Address in Block 6 above and the Old or Incorrect address below.

	_____
	Name
OLD ADDRESS	Organization
	_____
	Address
	City, State, Zip

(Remove this sheet, fold as indicated, staple or tape closed, and mail.)

END

DATE

FILMED

5-88

DTIC